



OsloMet – Storbyuniversitetet

Department of Civil Engineering and Energy Technology

Mailing address: PB 4 St. Olavs plass, N-0130 Oslo, Norway

Street address: Pilestredet 35, Oslo

Group No. 12

AVAILABILITY
Open

Phone: 67 23 50 00

www.oslomet.no

Master thesis

TITLE CFD Simulation of heavily insulated office cubicle heated by ventilation air	DATE 23. 05. 2018
	NUMBER OF PAGES/ATTACHEMENTS 54/5
AUTHOR Paulos Mekbib Kifle Tlf. 99874076	SUPERVISOR Habtamu Bayera Medessa
DONE IN COLLABORATION WITH ForKlima Project (SINTEF)	CONTACT Paulos Mekbib Kifle

ABSTRACT The thesis investigates the airflow and temperature distribution in an office cubicle which is heated by ventilation air using a ceiling mounted active supply air diffuser. Numerical simulation using STAR CCM+ has been implemented in order to understand the flow nature of air inside the office cubicle. A two equation k-ε model has been employed. The results show that the effect of supply air temperature has no significant effect for higher and medium flow rates (volumetric flow rates of 126 m ³ /h and 76 m ³ /h). Moreover, varying the volumetric flow rate of the supply air shows an increase in room temperature with decreasing volumetric flow rate. The simulation results have been validated with the available experimental data and shows good an agreement with an error less than 12 % for temperature and an error less than 6 % for velocity. The effect of additional heating element has also been studied. The results show a high velocity generation around a heating element resulting a significant reduction in thermal stratification.
--

3 KEYWORDS
Temperature distribution
Velocity distribution
CFD Simulation

Abstract

This thesis investigates the air flow and temperature distribution in an office cubicle which is heated by ventilation air using a ceiling mounted active supply air diffuser. Understanding the flow nature of air inside a room using analytical methods is more complex. Therefore, the use of a CFD simulation can be helpful for solving differential equations related to flow phenomena. For this master thesis, STAR CCM+ is used to simulate the airflow and temperature distribution in an office cubicle.

The study involves the solution of three-dimensional partial differentiation equations of conservation of mass, momentum, energy, turbulence kinetic energy and dissipation rate. The finite volume method and SIMPLE scheme with two equation k- ϵ turbulence model has been implemented to solve the governing differential equations numerically. The results show that the numerical simulations are in good agreement with an experimentally available data with an error less than 12 % for temperature and an error less than 6% for velocity.

Furthermore, ten different cases have been considered in this study. The effects of supply air temperature have shown no significant effect for higher and medium air flow rates (volumetric flow rates of 126 m³/h and 76 m³/h). However, for lower air flow rate (volumetric flow rates of 51 m³/h) it has been observed that supply air temperature influences the temperature profile and induces a clear temperature stratification, which shows higher temperature near to the ceiling, and lower temperature near to the floor. Moreover, varying the volumetric flow rate of the supply air has shown the room air temperature increases with a decrease in volumetric flow rate. The analysis of the effect of the outdoor temperature also suggests that the air flow and temperature distribution inside the room is affected by the outdoor temperature due to the heat transfer between the façade/window and the external temperature.

To investigate the effect of air diffuser types, two different ceiling mounted diffusers have been studied. The study shows that perforated type diffuser has created a better room air temperature with maximum operative air temperature of 25.4 °C. However, it generates a draught risk for occupant due to the high velocity inside the occupied zone.

The effect of having an additional heating unit has also been studied. The result shows that higher air velocity generated over the heating element flows upward along the vertical window

to the ceiling. In addition, thermal stratification of air inside the room has been reduced significantly.

It is concluded, that the validated CFD technique with k- ϵ turbulent model can be used for designing of the temperature and velocity distribution of a high energy efficient office buildings using mixed ventilation systems with ceiling mounted active diffuser.

Sammendrag

Hensikten med rapporten var å undersøke luftstrømning og temperaturfordeling i et cellekontor som er oppvarmet av ventilasjonsluft med en takmontert aktiv tilluftsventil. Å løse strømningsproblemer av luftstrøm inne i et rom er komplisert med analytiske metoder. Derfor kan bruk av numerisk væskedynamisk (CFD)- simulering være nyttig for å løse differensiallikninger relatert til luftstrømninger. For å løse problemstillingen er STAR CCM+ brukt for simulering av luftstrømningen og temperaturfordelingen inne i cellekontoret.

Studien innebærer løsningen av tredimensjonale partielle differensiallikninger for bevaring av masse, momentum, energi, turbulenskinetisk energi og spredningsrate. Kontrollvolummetoden og SIMPLE-ordningen med k - ϵ turbulensmodell ble brukt for å løse differensiallikningene. Simuleringsresultatene har vist at den numeriske beregningen samsvarer med de eksisterende målingsdata med mindre enn 12% avvik for temperatur og mindre enn 6% for hastighet.

Totalt ble det vurdert ti caser i denne studien. Variering av tilluftstemperaturen har ikke noe betydelig påvirkning for høyere og medium luftmengder (126 m³/h og 76 m³/h). Derimot, for lavere luftmengder (51 m³/h) har det blitt observert at tilluftstemperaturer påvirker temperaturprofilen og gir en klar temperatursjiktning: høyere temperatur nær taket, og lavere temperatur nær gulvet.

I tillegg er det vist en økning i romtemperatur ved reduksjon i tilluftsmengde.

For å vurdere påvirkning av forskjellige type tilluftsventiler er det blitt studert to forskjellige takmonterte ventiler. Resultatene viste at den perforerte tilluftsventilen har skapt bedre lufttemperatur i rommet med en maksimum operativ temperatur på 25.4 °C i oppholdssonen.

Påvirkningen av en ekstra varmeenhet har også blitt undersøkt. Resultatene har vist høyere lufthastighet generert over varmeenheten langs vinduet opp mot taket. I tillegg er temperatursjiktningen i rommet har blitt redusert betydelig.

Acknowledgments

This master's thesis has been carried out at the department of Civil Engineering and Energy technology , Oslo Metropolitan University, Oslo.

I am profoundly grateful to thank my advisor Habtamu Bayera for his extensive professional guidance and support for accomplishment of this study. The door was always open whenever I had a question about my research. His intensive follow up and supervision made this thesis.

I would like to express my gratitude to Arnab Chauduri, Mehrdad Rabani and Ole Melhus for their expertise specially for guiding me to solve problems in STAR CCM+, and I have learned a lot from them.

Most importantly, I would like to express my very proud gratitude to my loving and supportive wife Eskedar Gashaw and my three kids for providing me with unfailing support and continuous encouragement through my two years study process and writing this thesis. Finally, it would be a great pleasure to thank my friends Ayalew, Wondimagegn and Abushet for their encouragement and kind support in my two years journey. I would like to dedicate this work for my dear wife, this accomplishment would not have been possible without you. Thank you!

Table of Contents

Abstract	i
Sammendrag	iii
Acknowledgments	iv
List of Figures	viii
List of Tables	xi
<i>Nomenclature</i>	xii
1. Introduction	1
1.1. Objective	2
1.1.1. Sub - tasks	2
2. Theory	3
2.1. Ventilation strategies	3
2.2. Mixing ventilation	3
2.3. Displacement ventilation	5
2.4. Air flow pattern and throw	5
2.4.1. Air Jet	5
2.4.2. Non isothermal free jet	6
2.4.3. Jet flow formulae	7
2.5. Diffuser types	8
2.6. Ventilation effectiveness	9
2.7. Thermal comfort	9
2.7.1. Operative temperature	11
2.8. CFD modeling and numerical scheme	11
2.8.1. CFD model	11
2.9. Governing equations	12
2.9.1. Conservation law of fluid flow	12
2.9.2. Meshing	14

2.9.3.	Finite volume (or control volume) method	14
2.10.	Numerical scheme	15
2.10.1.	Upwind Scheme	15
2.10.2.	SIMPLE scheme.....	15
2.10.3.	Turbulence models	18
2.10.4.	K-Epsilon Turbulence	18
2.10.5.	K-Omega turbulent model.....	19
2.11.	Discretization method	19
3.	Methodology	20
3.1.	Geometry.....	20
3.2.	Mesh generation.....	22
3.3.	Physics and simulation models	24
3.3.1.	Reynolds-Average Navier-Stokes	25
3.3.2.	Relaxation.....	26
3.4.	Boundary conditions	27
3.5.	Convergence criteria	30
4.	Results and discussions	32
4.1.	Grid independence analysis	32
4.2.	Validation of CFD simulation with experimental data	33
4.3.	Parametric analysis	36
4.3.1.	Effect of supply air temperatures	36
4.3.2.	Effects of volumetric flow rate.....	46
4.3.3.	Effect of conventional heating element.....	49
4.3.4.	Effects of diffusers type	50
4.3.5.	Evaluation of ventilation efficiency	51
4.4.	Thermal comfort analysis	52
4.4.1.	Operative temperature	52

- 4.4.2. Vertical temperature difference..... 53
- 4.4.3. Draught rate..... 53
- 5. Conclusion and recommendation..... 54
- Appendix 1: Active supply air diffuser 58
- Appendix 2: Project execution plan 59
- Appendix 3: Velocity contour for different flow rates at outdoor temperature -1.8 °C 60
- Appendix 4 – Temperature and velocity profiles for different flow rates 61
- Appendix 5 : Velocity contours for different flow rates at outdoor temperature -10 °C..... 62

List of Figures

Figure 1:	An illustration for a horizontal throw, drop and Coanda effect (Engineers, 2011)	3
Figure 2:	Air flow pattern by displacement ventilation with internal thermal load (Peter V. Nielsen, 1995)	5
Figure 3:	Illustration of jet flow (GANGISETTI, 2010)	6
Figure 4:	2D distribution of stream line at different Archimedes number. (Peter V. Nielsen, 1995)	7
Figure 5:	A trajectory of a horizontal free jet (Peter V. Nielsen, 1995)	8
Figure 6:	Active diffuser type TTC-250 (a) assembly and (b) section drawing showing detail inside (LINDVENT)	8
Figure 7:	Swegon ceiling mounted perforated diffuser type COLIBRI free (Swegon)	9
Figure 8:	Steps in CFD simulation	12
Figure 9:	Conservation of general fluid flow variable (H K Versteeg 2007)	15
Figure 10:	Computational sequence of SIMPLE algorithm (Versteeg & Malalasekera, 2007)	17
Figure 11:	Schematic showing the dimensions, locations of an air supply diffuser, an exhaust diffuser, lights, a human simulator, a pc, and a heating element.	21
Figure 12:	Visual illustration of mesh domain with fine mesh near the inlet, outlet, human simulator and PC	23
Figure 13:	Procedure in generating automated mesh, volume control and surface control	23
Figure 14:	Physics models selected for the simulation	25
Figure 15:	Schematic showing the boundary conditions employed	28
Figure 16:	Room configuration and measuring probes layout (P1, P2, P3 & P4) measuring poles and PC and human simulator	30
Figure 17:	Converged residual for flow rate 177 m ³ /h simulation	31
Figure 18:	Comparison of temperature and velocity profile for three different mesh sizes	33
Figure 19:	Comparison of simulation results with experimental data reported by Axel et al (Axel et al., 2015)	34
Figure 20:	Temperature distribution on plane A & B at different temperatures for case 2 with volumetric flow rate of 126 m ³ /h for external temperature of -1.8 °C.	37
Figure 21:	Velocity contour for case 2 at different temperatures	38
Figure 22:	Vertical temperature profiles at different temperatures for (a) 126 m ³ /h (b) 76 m ³ /h (c) 51 m ³ /h	38

Figure 23: Temperature and velocity distribution on plane A for case 3 at different temperatures with volumetric flow rate 76 m ³ /h for external temperature of -1.8 °C.....	39
Figure 24: Temperature and velocity distribution for different temperature for flow rate 51 m ³ /h for external temperature of -1.8 °C.	41
Figure 25: Temperature and velocity distribution for case 5 (126 m ³ /h) for different temperatures at external temperature (-10 °C).....	43
Figure 26: Temperature and velocity distribution for case 6 (76 m ³ /h) at different temperature external temperature (-10 °C)	44
Figure 27: Temperature distribution and velocity vector for case 7 (51 m ³ /h) for different temperature at external temperature (-10 °C)	46
Figure 28: Temperature distribution inside the room for different volumetric flow rates.....	47
Figure 29: Temperature contour for cases 1 (177 m ³ /h),2 (126 m ³ /h),3 (76 m ³ /h) and 4 (51 m ³ /h).	48
Figure 30: Velocity contours for different volumetric flow rates	48
Figure 31: Temperature contour and velocity vector for flow rate 51 m ³ /h and temperature of 26 °C (a) & (b) with radiator (c) & (d) with out radiator	50
Figure 32. Temperature & velocity distribution along plane A for case 9 active diffuser (a) & (b) and perforated diffuser (c) & (d)	51
Figure 33: Vertical temperature profile and velocity profile for two different diffusers (case 9).....	51
Figure 34: Product description for active supply diffuser	58
Figure 35: Velocity contour for flow rate of 76 m ³ /h at supply air temperatures (a) 24 °C, (b) 26 °C and (c) 28 °C at outdoor temperature of -1.8 °C	60
Figure 36: Velocity contour for flow rate of 51 m ³ /h at supply air temperatures 24 °C, 26 °C and 28 °C at outdoor temperature of -1.8 °C	60
Figure 37: Temperature and velocity profile for flow rates 126 m ³ /h different supply temperature for outdoor temperature of - 1.8 °C and 10 °C.....	61
Figure 38: Temperature and velocity profile for flow rate 76 m ³ /h different supply temperature for outdoor temperature of - 1.8 °C and 10 °C.....	61
Figure 39: Velocity contour of flow rate 126 m ³ /h for different supply air temperatures at outdoor temperature of -10 °C.	62
Figure 40: Velocity contour of flow rate 76 m ³ /h for different supply air temperatures at outdoor temperature of -10 °C.	62

Figure 41: Velocity contour of flow rate 51 m³/h for different supply air temperatures at outdoor temperature of -10 °C 63

List of Tables

Table 1:	A detail explanation of the effect of inlet and outlet position in mixing ventilation (Cao et al., 2014).	4
Table 2:	Shows the categorization of a recommended areas for PPD and PMV (Standard, 2014).....	10
Table 3:	Description of the geometry with dimensions and position.....	21
Table 4:	Parameter values for supply diffuser and exhaust diffusers employed for mesh refining during automated meshing.....	24
Table 5:	Boundary conditions used for CFD model of the cubicle office	29
Table 6:	Selected cases for numerical simulation	32
Table 7:	Comparison of mass flow rate and heat transfer for three different mesh sizes	33
Table 8:	Quantitative comparison of temperature distribution between measured and simulated result for Validation	35
Table 9:	Vertical air temperature difference in occupied zone between 0.1 m and 1.7 m for different supply air temperature and flow rates.....	41
Table 10:	Surface average temperatures for the room volume	52
Table 11:	project execution plan for the master's thesis.....	59

Nomenclature

Greek symbols

ρ	density of air [kg/m ³]
τ	air change time [s]

Latin symbols

K	Jet model coefficient [-]
Re	Reynolds number [-]
AR	Archimedes number [-]
To	turbulent intensity [%]
u	Magnitude of air velocity [m/s]
V	Volume of the room [m ³]
A	Area of the room [m ²]
q	The volumetric flow rate [m ³ /s]
k	Turbulent kinetic energy [m ² /s ²]
a _o	area of the supply diffuser [m ²]
u _o	wall velocity [m/s]
β	Coefficient of thermal expansion [1/K]
g	Gravitational acceleration [m/s ²]
ΔT	temperature difference between the supply and exhaust
I _o	momentum of flow
t	time [s]
M	Metabolism [W/m ²]
W	External work [W/m ²]
F	View factor [-]

Subscript

e	Exhaust
---	---------

s	Supply
i	Inlet
p	Pollutant
mr	mean radiant

Abbreviations

HVAC	Heat, Ventilation, Air Conditioning
CFD	Computational Fluid Dynamics
PPD	Predicted Percentage Dissatisfied
PMV	Percentage Mean Vote
PD	Percentage Dissatisfied
CAD	Computer Aided Design
RANS	Reynolds-Averaged Navier-Stokes
SIMPLE	Semi Implicit Method for Pressure-Linked Equations
LES	Large Eddy Simulation
DES	Detached Eddy Simulation
SST	Shear Stress Transport with Gamma ReTheta Transition
GCI	Grid Dependence Index
RSM	Reynolds Stress Model

1. Introduction

Energy consumption in buildings has been a big concern among researchers in the last decades owing to environmental issues and cost of energy. The energy consumption in buildings in Europe is estimated around 40% of the total energy (cao.2016). The Strict requirements in building's high energy performance and energy effectiveness has resulted in a low heating power demand owing to well insulated façade, high air tightness, and the application of demand controlled ventilation systems. To achieve this goal the Energy Performance of Buildings Directive (EPBD) 2010/13 (Union, 2012) has outlined new buildings of the European Union member states must have nearly zero-energy buildings by the end of 2020. In order to save the energy consumption of modern buildings it is recommended to use demand controlled ventilation systems.

Ventilation is used in buildings to create an indoor environment with an acceptable air quality and thermal comfort. In order to create a favourable thermal environment inside an energy efficient building, heating using a warm ventilation air can be an option over the conventional heating systems. However, it is important to investigate the effects of heating by using ventilation air based on the thermal comfort of occupants in the ventilated room.

The main purpose of having an HVAC system in a building is to create a better thermal comfortable environment for occupants. Therefore, it is important to study the performance of the ventilation air distribution inside the room.

The analysis of room air heated by a hot supply jet requires coupling of energy equation along with momentum and continuity equation for the determination of the flow field and temperature distribution inside a room. The complexity in the flow nature of the room air, makes the determination of the analytical solutions of the governing differential equation difficult (Qasim, Sabah, & Ala'a Abbas, 2014). Therefore a numerical approach using Computational Fluid Dynamic (CFD) simulation is required to solve the Navier- Stokes equation and predict the air flow pattern in the room. Moreover, CFD gives a spatial information giving values for the flow variables in the room domain (Qasim et al., 2014). Now a days an advancement in the area of the CFD modelling has made the air flow modelling in a room simple and conceivable. Among different commercial CFD tools STAR - CCM+, and ANSYS - FLUENT are most widely used in academic world.

The main objective of this study is to investigate the air flow and temperature distribution using a numerical tool in an office cubicle which is heated by warm ventilation air. In addition to this

assessing whether it is possible to cover the heating demand with warm ventilation air exclusively during the coldest days without affecting thermal comfort for occupants.

1.1. Objective

The main objective of this study is to investigate and analyse the effects of ceiling diffusers in an office cubicle designed according to the Norwegian passive house standard. The office cubicle is primarily heated by ventilation air. And the project as well investigates the effect of conventional heating on the temperature and velocity profile of the room air.

The study is mainly focused on numerical simulation and the Computational Fluid Dynamics (CFD) tool STAR CCM+ is used for this purpose.

1.1.1. Sub - tasks

This section describes the detailed objectives of the master thesis as stated below.

- Detail literature review about ventilation based heating systems for an office building.
- Understand the use of STAR CCM+ software
- Numerical investigation of velocity and temperature distribution of ventilation air in an office cubicle heated by ventilation air, and validate the results with existing experimental data.
- Conduct a parametric analysis on the following cases:
 - Effect of supply air temperature and volumetric flow rate
 - Effect of conventional heating power
 - Effect of turbulent models
 - Effect of diffuser types.

2. Theory

This chapter focuses on the basics of the ventilation strategies and the CFD modelling and numerical simulation scheme, underlying physics of fluid flow and heat transfer, the discretization of the governing equations, and means of preparing and discretizing the geometry.

2.1. Ventilation strategies

2.2. Mixing ventilation

The basic principle of the mixing ventilation is a dilution of contaminants concentration by bringing in outdoor air into the occupied zone through a high impulse air stream. According to the study, which was conducted by Cao (2014) location of air supply and return has a strong impact on the air distribution in a mixing ventilation (Cao et al., 2014). With mixing ventilation strategy, the occupied zone can be ventilated either by direct drop or by the return flow of the supplied jet. In both cases, a good throw of the supply air gives a good mixing in the room. A throw is a horizontal or vertical distance an air stream travels after it leaves the air outlet, usually assumes the surface adjacent to the air outlet.

A ceiling mounted supply air diffuser gives an advantage of the Coanda effect of air sticking to a surface to increase the throw of the supply air. The Coanda effect is a low-pressure area that develops between the air stream and the ceiling, allowing the air stream to travel along the ceiling and further increasing the throw (Alan Budrik, December 2011) as shown in figure 2.

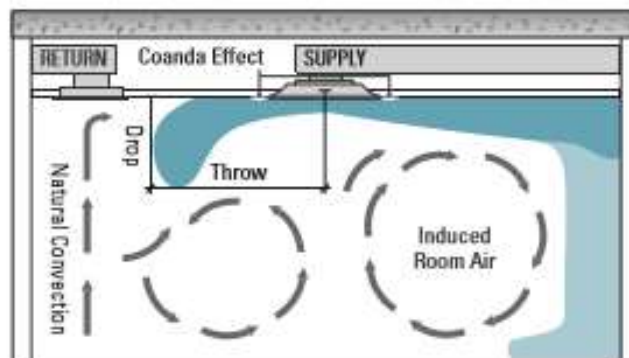


Figure 1: An illustration for a horizontal throw, drop and Coanda effect (Engineers, 2011)

Cao et al (2014) has summarized the effects of the diffuser locations in air mixing from different scientific studies as shown in the table 1 (Cao et al., 2014). The study included both experimental and numerical studies.

Table 1: A detail explanation of the effect of inlet and outlet position in mixing ventilation (Cao et al., 2014).

	Locations of airflow inlet and outlet	Methods	Main focus	Findings
Boyle Son (1899) [19]		Investigation	Airflow distribution and indoor air quality.	<ul style="list-style-type: none"> This is one of the very earliest forms of mechanical ventilation Downdraught ventilation by mechanical impulsion is pronounced by public health experts to be highly prejudicial to health.
Clements (1975) [14]		Model experiment	Airflow pattern and the effect of Archimedes number.	<ul style="list-style-type: none"> The air pattern is almost a function of the Archimedes number. As Ar increases, the jet deflection from the horizontal increases.
Sandberg et al. (1986) [25]		Experimental study	Air exchange efficiency and contaminant exposure.	<ul style="list-style-type: none"> The ceiling-to-floor system gives rise to a comparatively rapid exchange of the air with heating. However, the evacuation of the contaminant is delayed.
Nielsen (1991) [111]		Modeling and experimental study	Simplified design method.	<ul style="list-style-type: none"> Simplified design models work well with simple geometry Measurements show significant deviation.
Sandberg et al. (1992) [26]		Experimental study	The effect of Archimedes number on the airflow distribution.	<ul style="list-style-type: none"> The critical supply Archimedes number at which the jet breaks away from the surface as soon as it leaves the nozzle was just below 0.03.
Awbi and Gan (1993) [27]		Numerical study	Air distribution and ventilation effectiveness.	<ul style="list-style-type: none"> Air distribution systems should be different for heating and cooling in order to achieve a comfortable room environment.
Lee and Awbi (2004) [28]		Experimental and numerical study	The effects of partitions on the room air quality as well as ventilation performance.	<ul style="list-style-type: none"> Increasing the partition gap underneath from 0.2H to 1.02H causes an overall improvement in the air change efficiency.
Cao et al. (2010) [29]		Experimental study	Maximum velocity decay in the air distribution via attached plane jet.	<ul style="list-style-type: none"> Attached plane jet can be used as an effective method to avoid draught in mixing ventilation conditions.
Krajčičk et al. (2012) [33]		Experimental study	Air distribution and ventilation effectiveness.	<ul style="list-style-type: none"> The ventilation effectiveness varied between 0.4 and 1.2, where 1 is complete mixing, which depends on the position of air terminal devices.

2.3. Displacement ventilation

The principle of displacement ventilation supplies fresh air with low speed (typically <0.5 m/s) (Cao et al., 2014) from the bottom of the room and eliminating thermal loads and pollutant concentration from the occupied zone. Airflow moves up slowly in a kind of the piston flow with the help of buoyancy. The plumes from the heat sources lift the air up and create a natural convection flow upwards in the room and it exhausted at the highest level, see figure 2. This type of air distribution is effective at delivering fresh air to occupants and removing contaminants associated with heat sources. While creating a comfortable environment. However, this type of ventilation systems usually create a vertical gradient of air velocity, temperature and contaminants concentration (Tomasi, Krajčik, Simone, & Olesen, 2013).

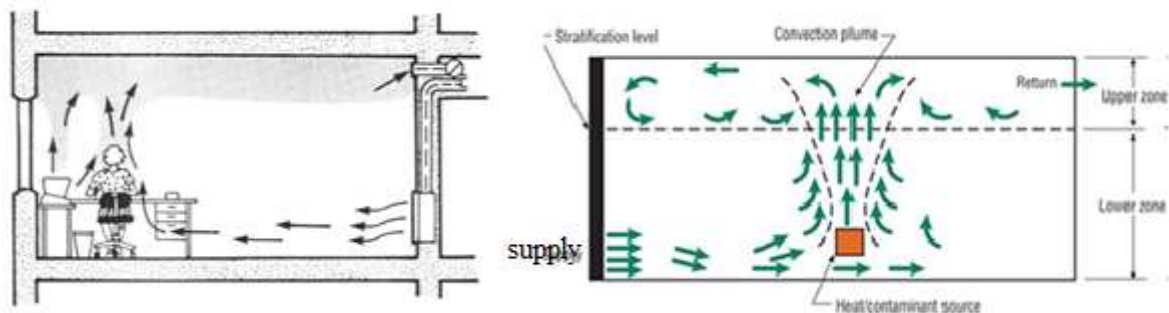


Figure 2: Air flow pattern by displacement ventilation with internal thermal load (Peter V. Nielsen, 1995)

2.4. Air flow pattern and throw

In the air flow pattern, the air velocity vectors show the path followed by air particles, and the pattern depends up on the type of diffusers, location of diffuser, jet momentum and jet direction. (GANGISETTI, 2010).

Air throw represents the distance from the centre of the supply diffuser face to a point where the velocity of the air stream is reduced to a specified velocity, usually 0.75 m/s, 0.50 m/s or 0.25 m/s (Engineers, 2011). The air throw is the function of mass flow rate and the outlet velocity therefore can be either decreased or increased by changing either of these values. The throw length is usually given in manufacturer's catalogue.

2.4.1. Air Jet

Air jet can be classified as free jet if it is not obstructed by ceilings or walls, and isothermal jet if the air flow temperature is the same as the ambient temperature in the room or non-isothermal jet if the air flow temperature is different from the ambient temperature.

Based on the previous studies made air jet can be divided it to four sections in terms of its center line velocity decay as shown in figure 3. Core zone is an immediate area outside the diffuser opening where the core velocity U_0 is equal to the core or initial velocity. It usually extends approximately four diameter from the supply opening. Transitional zone extends to the secession of four diameter of length for turbulence flow occurs, in this zone the centerline velocity, U_x , is inversely proportional to \sqrt{x} where x is the distance from the plane of the outlet. The main region, turbulent flow is fully established and the influence of inertial force predominates and it extends a length of 25 -100 equivalent outlet diameter. U_x is proportional to $\frac{1}{x}$. Terminal zone- is the end of the turbulent region and the velocity decay is very rapid and it is in the order of less than 0,25 m/s (Jones, 1997).

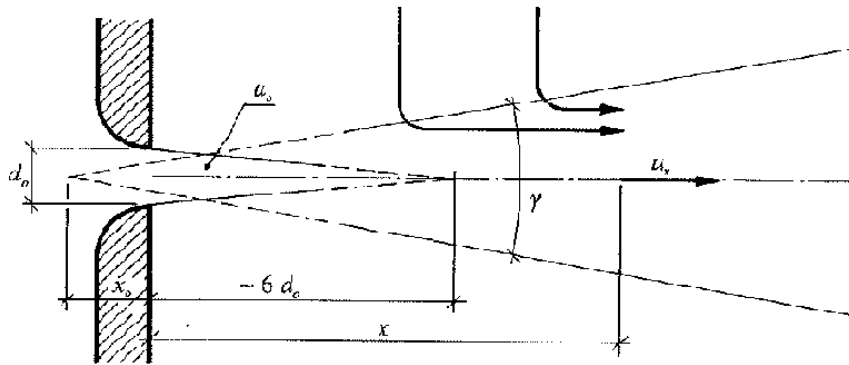


Figure 3: Illustration of jet flow (GANGISETTI, 2010)

A wall jet has theoretically have a constant velocity u_0 everywhere at the opening (top hat profile) and therefore it is the momentum flow from the opening which controls the movement in case of mixing ventilation and it is given by the equation:

$$I_o = \rho_o a_o u_o^2 \quad 1$$

where ρ_o and a_o are density and supply area respectively (Peter V. Nielsen, 1995)

2.4.2. Non isothermal free jet

The buoyancy will influence the flow in a jet if air is supplied with a temperature different from the return air temperature to the room. The flow is characterized by the Archimedes number Ar (Peter V. Nielsen, 1995), which compares the relative strength of buoyancy force in the room to the momentum of the supply jet air flow.

Thermal stratification inside a room depend on the Archimedes number. Several studies have shown that air flow pattern in the room is mainly dependent on the Archimedes number and it can be given as the ratio between Grashof's number and Reynolds number as ($Ar \approx \frac{Gr}{Re^2}$), thus combines the effect of natural convection due to buoyancy and forced convection due to the supply air jet (STARCCM+, 2017).

$$Ar = \frac{g\beta l_o \Delta T_o}{u_o^2} \tag{2}$$

where g , β , ΔT and l_o are the gravitational acceleration, coefficient of thermal expansion, temperature difference between return and supply air and characteristic length respectively. The characteristic length l_o can be expressed as $\sqrt{a_o}$ for flow from ceiling mounted diffusers and h_o in case of jet flow from a slots (Peter V. Nielsen, 1995).

Nielsen also showed in his study the effects of Archimedes number in the distribution of stream line and direction of recirculating cold supply jet in the room as illustrated in figure 4 (Peter V. Nielsen, 1995).

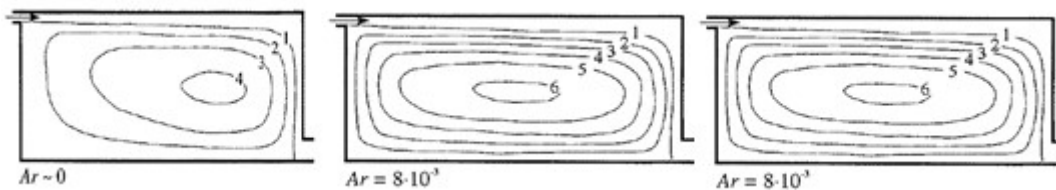


Figure 4: 2D distribution of stream line at different Archimedes number. (Peter V. Nielsen, 1995)

2.4.3. Jet flow formulae

For the fully developed flow region jet formulae specify the jet velocity and temperature profiles, trajectory and jet decay. The momentum flow is preserved from the free jet because it is assumed that the direction of entrainment is perpendicular to the flow direction. Circular jet width increase linearly to a distance of $+x_o$, that means the area of a jet will increase with the square of the distance. The momentum flow equation shows that for at momentum is preserved the velocity is inversely proportional to the distance and can be written as (Peter V. Nielsen, 1995)

$$\frac{u_x}{u_o} = \frac{K_a}{\sqrt{2}} \frac{\sqrt{a_o}}{x+x_o} \tag{3}$$

Where $\frac{u_x}{u_o}$ is dimensionless velocity ratio, $\frac{\sqrt{a_o}}{x+x_o}$ is dimensionless distance ratio, a_o is area of the supply opening and K_a is a constant for different types of diffusers and constant in case of high turbulent flow

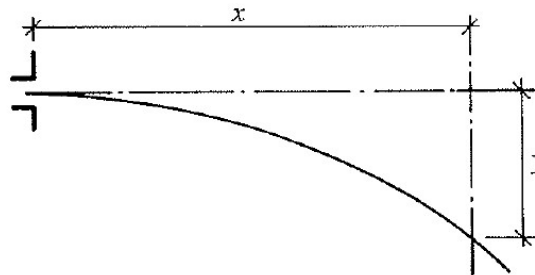


Figure 5: A trajectory of a horizontal free jet (Peter V. Nielsen, 1995)

2.5. Diffuser types

In order to supply afresh air to the room it is important to select an appropriate type of diffuser. There are different diffuser types in the market depending up on the types of ventilation strategies and the applications. Among these an active ceiling diffuser is the type which is equipped with electronic sensors for demand control of air flow and climate control. It gives to the users an acceptable thermal comfort by the an adjustable vertical moving slots. An active supply diffuser has six slots which is moving long guide vane in order to control the supply of air with regards to the demand inside the room. Figure 6 is an illustration of an active supply diffuser type TTC – 250.



Figure 6: Active diffuser type TTC-250 (a) assembly and (b) section drawing showing detail inside (LINDVENT).

A ceiling mounted perforated supply air diffuser type from Swegon is an example. The diffuser has a circular geometry with a removable diffuser face figure 7 is an illustration of perforated diffuser.



Figure 7: Swegon ceiling mounted perforated diffuser type COLIBRI free (Swegon)

2.6. Ventilation effectiveness

In different studies ventilation effectiveness is defined as the measure of the air exchange rate, removal of pollutant, heat removal and air distribution index (Amai. Thesis 2016). However, Hdeyuki Amai & Alila Novoselac defined ventilation effectiveness in terms of heat removal (Amai & Novoselac, 2016), and can be given a the temperature effectiveness (ϵ_T) :

$$\epsilon_T = (T_S - T_E) / (T_S - T_O) \quad 4$$

where T_S the supply air temperature, T_E the exhaust air temperature and T_O the average room air temperature (Amai & Novoselac, 2016). Usually, the value of ϵ_T is $<100\%$ for mixing ventilation and $>100\%$ for displacement ventilation (Gan, 1993). A vlue for $\epsilon_T \leq 1$ is an implication of som amount of cold supply air in the room which is not mixed with the room air and leaving the exhaust. The temperature effectiveness is considered to be effective when it is $\epsilon_T \geq 1$ (Kharagpur).

2.7. Thermal comfort

Thermal comfort is defined as the state of mind of occupants expresses satisfaction with the environment. The most effective tools to measure the thermal comfort level in the surrounding environment is to measure the variables that trigger discomfort and the body's response to it (Syed, 2012).

The primary factors that must be addressed when defining conditions of thermal comfort aer metabolic, clothing insulation (Icl), air temperature in the indoor environment, mean radiant temperature, air speed and relative humidity rate (Miroshnichenko & Sheremet). Among the number of thermal comfort models available, the index developed by Fangers (1970) used predicted mean vote (PMV) and predicted percentage dissatisfied (PPD) to assess body heat exchange with the environment and thermal comfort. It is also common to measure thermal

comfort with temperature distribution, percentage of dissatisfied people due to draft (PD) as given in equation (18). The calculation of PMV which is given by the equation (11) and PPD which is given by the equation (17) is based on ISO 7730 and the equation is based on the empirical investigation of how different healthy people react for indoor environment where thermal comfort is desirable. PPD indexes establish a quantitative prediction of the percentage of thermally dissatisfied people who feel too hot or too cold (Standard, 2005). The predicted mean vote (PMV) is an index that predict mean value of vote form large group of people in 7 points in the range of -3 (representing a response for cold) 0 (representing a thermally neutral) to +3.

$$PMV = (0.303 \cdot e^{-0.036M} + 0.028) \cdot [(M - W) - H - E_c - C_{res} - E_{res}] \quad 5$$

Where M is metabolism (W/m²), W is external work (W/m²), h_c is the convective heat transfer coefficient (W/m².K), and Pa is the water vapor partial pressure (Buratti, Palladino, & Moretti), v_{av} is the average air velocity [m/s] (Standard, 2005).

PPD can also be calculated with the PMV value determined by equation (11) using the equation (Standard, 2005):

$$PPD = 100 - 95 \cdot \exp(-0,03353 \cdot PMV^4 - 0,2179 \cdot PMV^2) \quad 6$$

According to the standard NS-EN 15251 it is also recommended to categorize an occupant's thermal comfort and percentage discomfort in to four when designing an air handling units. The table.2 below shows the categories and the expected average thermal assessment

Table 2: Shows the categorization of a recommended areas for PPD and PMV
(Standard, 2014)

Category	Thermal conditions for the entire building	
	PPD [%]	Expected average assessment
I	<6	-0,2 < PMV < +0,2
II	<10	-0,5 < PMV < +0,5
III	<15	-0,7 < PMV < +0,7
IV	>15	PMV < -0,7; or +0,7 < PMV

2.7.1. Operative temperature

Operative temperature is the weighted average temperature for convection and radiation between a person and the surrounding environment to the combined heat transfer coefficient. It is calculated from the average of mean radiant temperature and air temperature.

$$T_o = \frac{T_{mr} + T_a}{2} \quad 7$$

Where T_a air temperature and T_{mr} mean radiant temperature.

The mean radiant temperature is an important factor in the thermal comfort equation which is an influence of the surface temperatures, area, geometric position, posture and facing orientation of the occupant with respect to a certain decided point. If the temperatures for a given surfaces are known mean radiant temperature can be calculated in a simplified equation:

$$T_{mr} = F_1 T_1 + F_2 T_2 + \dots + F_n T_n \quad [\text{K}] \quad 8$$

F_n – is view factor for surface n

T_n – is temperature of surface n [K]

In addition the vertical air temperature gradient between head and feet of the seated or standing person should be kept below 3 °C (Standard, 2005).

2.8. CFD modeling and numerical scheme

2.8.1. CFD model

Computational fluid dynamics (CFD) is used to study systems involving fluid flow, heat transfer and chemical reactions by means of computer-based simulation (Versteeg & Malalasekera, 2007). In CFD codes there are three major steps involved: Pre-processor, Solver and Post-processing. Pre-processor includes the definition of problem and creation of the flow domain by using geometry construction and grid generation. Solver refers to the selection of physical models, definition of fluid properties, specification of appropriate boundary conditions and solutions of flow equations. Post-processor refers to visualization of the flow variables and interpretation of the predicted results

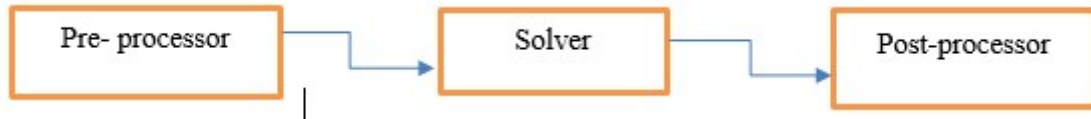


Figure 8: Steps in CFD simulation

CFD provides the capability to investigate the complex flow structures and provide detailed results at every point in the flow domain. Figure 8 shows the steps in CFD simulation. The CFD software is dividing the enclosure into a cell or controlled volumes. The accuracy of the CFD simulations depends on how accurate the boundary conditions are set and on the numerical simulation parameters. STAR CCM+ software solves the 3D Reynolds Navier-Stokes equations of mass- averaged velocity and time averaged pressure, energy and density. The fluid flow solver, STAR CCM+ in this work provides the solution comprised of a 3D, steady/transient, incompressible/compressible flow, laminar/turbulent fluid flow in a complex geometry.

2.9. Governing equations

2.9.1. Conservation law of fluid flow

Air flow and temperature in the room are described by the conservation law of mass, momentum and energy, in which the flow is assumed to be steady-state three dimensional incompressible and turbulent. The buoyancy effect is included in the momentum equation, and density is treated by the incompressible ideal gas law that is only varies with the temperature. The conservation law of physics is defined by Versteeg and Malalasekera (Versteeg & Malalasekera, 2007) which is applied on three fundamental quantities of the physical behaviors of fluid flow inside an enclosure : momentum, energy and mass of fluid particles.

The governing conservation equation for a general variables:

$$\frac{\partial(\rho\phi)}{\partial t} + \mathbf{div}(\rho\phi\mathbf{u}) = \mathbf{div}(\Gamma \mathbf{grad} \phi) + \mathbf{S}_\phi \quad 9$$

This can be written in Cartesian coordinate as:

$$\partial \frac{(\rho\phi)}{\partial t} + \frac{\partial(\rho u\phi)}{\partial x} + \frac{\partial(\rho v\phi)}{\partial y} + \frac{\partial(\rho w\phi)}{\partial z} = \frac{\partial}{\partial x} \left(\Gamma \frac{\partial\phi}{\partial x} \right) + \frac{\partial}{\partial y} \left(\Gamma \frac{\partial\phi}{\partial y} \right) + \frac{\partial}{\partial z} \left(\Gamma \frac{\partial\phi}{\partial z} \right) + \mathbf{S}_\phi \quad 10$$

Where ϕ is the transport coefficient which is independent variables: the mass or mole fraction in conservation of mass, velocity for conservation of momentum and enthalpy or temperature for conservation of energy, Γ is diffusion coefficient and \mathbf{S}_ϕ source term can be gravitational force.

When ϕ is unity, the equation represents conservation of mass.

Integration of the differential equation.23 over the corresponding finite volume and substitution of each term with discrete values ϕ in the nodal points gives the formula:

$$\mathbf{a}_p \phi_p = \sum_{nb=E,W,S,N} \mathbf{a}_{nb} \phi_{nb}^{n+1} + \mathbf{b}^n \quad 11$$

Where n is the number of iteration, nb is neighboring coefficient, b is the source term and ϕ is the discrete value of the dependent values over the control volume.

The governing conservation equation could be solved with regards to the different fluid particle sizes (ϕ) which is mass or mole fraction for conservation of mass, temperature and enthalpy for conservation of energy and velocity for conservation of momentum. The governing conservation equation can be solved for each nodes.

$$\frac{\partial \rho}{\partial t} + \frac{\partial(\rho u)}{\partial x} + \frac{\partial(\rho v)}{\partial y} + \frac{\partial(\rho w)}{\partial z} = 0 \quad 12$$

Where ρ , u , v and w are fluid density and fluid particle velocities in the x, y and z axis in the time t

Equation (7) is for unsteady state three dimensional mass conservation or continuity equation at a point in a compressible fluid. While for incompressible (the density is constant) steady state condition the conservation of mass equation becomes (Versteeg & Malalasekera, 2007)

$$\frac{\partial \rho}{\partial t} + \text{div}(\rho u) = 0 \quad 13$$

$$\frac{\partial u}{\partial x} + \frac{\partial v}{\partial y} + \frac{\partial w}{\partial z} = 0 \quad 14$$

Conservation of momentum:

The momentum equation (Navier Stoke equation) is derived throughout flow domain as,

$$\rho V \cdot \nabla V = -\nabla_p + \mu \nabla^2 V + \rho g$$

$$\frac{\partial(\rho v)}{\partial t} + \nabla \cdot (\rho v v) = -\nabla \cdot (PI) + \nabla \cdot T_t + F \quad 15$$

where P is pressure, F body force and T is viscous stress tensor which is given by (STARCCM+, 2017)

$$T_t = 2\mu_t S - \frac{2}{3}(\mu_t \nabla \cdot \bar{v})I \quad 16$$

Where S it the mean strain rate tensor, \bar{v} is the mean velocity and I is the identity tensor or the tensor of unity

Conservation of energy:

For energy equation in three dimension, four terms are associated with energy change in fluid particle. (Versteeg & Malalasekera, 2007)

$$\begin{aligned} \frac{\partial DE}{Dt} = -\text{div}(\rho u) + & \left[\frac{\partial(u\tau_{xx})}{\partial x} + \frac{\partial(u\tau_{yx})}{\partial y} + \frac{\partial(u\tau_{zx})}{\partial z} + \frac{\partial(v\tau_{xy})}{\partial x} + \frac{\partial(v\tau_{yy})}{\partial y} + \frac{\partial(v\tau_{zy})}{\partial z} + \frac{\partial(w\tau_{xz})}{\partial x} + \frac{\partial(w\tau_{yz})}{\partial y} + \right. \\ & \left. \frac{\partial(w\tau_{zz})}{\partial z} + \text{div}(k \text{ grad } T) + S_E \right] \end{aligned} \quad 17$$

The governing equation is the same for all indoor environment application of airflow and heat transfer, but the boundary condition changes for each specific physical problems (Qingyan & Srebric, 2002).

2.9.2. Meshing

Meshing is one of the most important part of the CFD simulation in which the flow equations depends on. The mesh represents how the computational domain discretized into a finite number of control volume. All of the control volume collectively make up the simulation's computational domain. Due to the direct dependence of the fluid variables computed by each model simulations on discretized meshes, the distribution and the refinement of the discretized cells is fundamental to a simulation's ability to accurately predict the physics and fluid flow occurring within the computational domain (Iverson, 2013).

It may be computationally expensive and needs long computational time to use a very fine mesh size, but it ensures that the solution is very accurate. However a higher resolution should be applied regardless of the computational time in the areas of flow plums above heat sources.

2.9.3. Finite volume (or control volume) method

In this section, it is presented the different numerical methods used to compute the fluid flow. Among the three distinct stream of the numerical solution techniques finite volume method is most widely applied computational fluid dynamics solution now a days. Finite volume method is based on the discrete version of the integral form of the conservation equation of fluid flow applied to each control volume (STARCCM+, 2017). Once the geometry was meshed and divided into small cells which is also called control volume, the integrated governing equations of fluid flow within computational domain are satisfied with conservation of each relevant properties for the control volume.

The conservation of general flow variable Φ , e.g. a velocity component or enthalpy, with in a finite control volume can be expressed as a balance in words:

$$\left[\begin{array}{l} \text{Rate of change} \\ \text{of } \phi \text{ in the} \\ \text{control volume} \\ \text{with respect to} \\ \text{time} \end{array} \right] = \left[\begin{array}{l} \text{Net rate of} \\ \text{increase of } \phi \\ \text{due to convection} \\ \text{into the control} \\ \text{volume} \end{array} \right] + \left[\begin{array}{l} \text{Net rate of} \\ \text{increase of} \\ \phi \text{ due to} \\ \text{diffusion into} \\ \text{the control} \\ \text{volume} \end{array} \right] + \left[\begin{array}{l} \text{Net rate of} \\ \text{creation of} \\ \phi \text{ inside the} \\ \text{control} \\ \text{volume} \end{array} \right]$$

Figure 9: Conservation of general fluid flow variable (H K Versteeg 2007)

As per the figure 8 the total net change of the key transport phenomena convection, diffusion and source terms is contained in change control volume in time. In STAR CCM+ finite volume method is applied.

2.10. Numerical scheme

Numerical method for calculating air flow behavior and heat transfer performance is getting a more and more beneficial approach than the corresponding experiments. It is saves both time and money. Among with the multi-field applications, numerical simulation of the internal air flow pattern inside buildings is developer rapidly in recent years. The quality of the CFD simulation can depend on various factors such as proper mesh, models, boundary conditions and numerical procedures.

2.10.1. Upwind Scheme

The main advantage of upwind differencing scheme is its ability to identify flow direction apart from central differencing. The upwind differencing or 'donor cell' differencing scheme takes in to account the flow directions when determining the value at a cell face: the convected value of ϕ at a cell face is taken to be equal to the value at the upstream node.(Versteeg & Malalasekera, 2007)

2.10.2. SIMPLE scheme

STAR CCM+ implements SIMPLE for pressure and velocity coupling schemes in solution methods. SIMPLE stands for Semi-Implicit Method for Pressure-Linked Equations. To initiate the SIMPLE calculation a pressure field p^* and velocities u^* and v^* are guessed. New pressure correction p' and velocity components correction u' and v' are introduced to obtain iteratively new, improved pressure p^{new} and velocity components u^{new} and v^{new} as written in the following equations: (Versteeg & Malalasekera, 2007)

$$p^{new} = p^* + \alpha_p p' \quad 18$$

$$u^{new} = \alpha_u u + (1 - \alpha_u)u^{(n-1)} \quad 19$$

$$v^{new} = \alpha_v v + (1 - \alpha_v)v^{(n-1)} \quad 20$$

Where α is under-relaxation factor for pressure and velocity? The value of α is between 1 and 0 to move the iterative improvement process forward, but small enough to ensure computational stability. If α equals 1 the pressure and velocity correction is far away the final solution. Where as when the value of α is zero there would apply no correction to the computation. (Versteeg & Malalasekera, 2007)

Versteeg and W Malalasekera gives in the following figure 10 the sequence of operation in the CFD procedure which employs the SIMPLE scheme.

First-order upwind discretization scheme was considered for pressure, momentum, turbulent kinetic energy, turbulent dissipation energy, and energy equations because it provides fast convergence and better results in the flow field and temperature distribution. (S.P. Corngati)

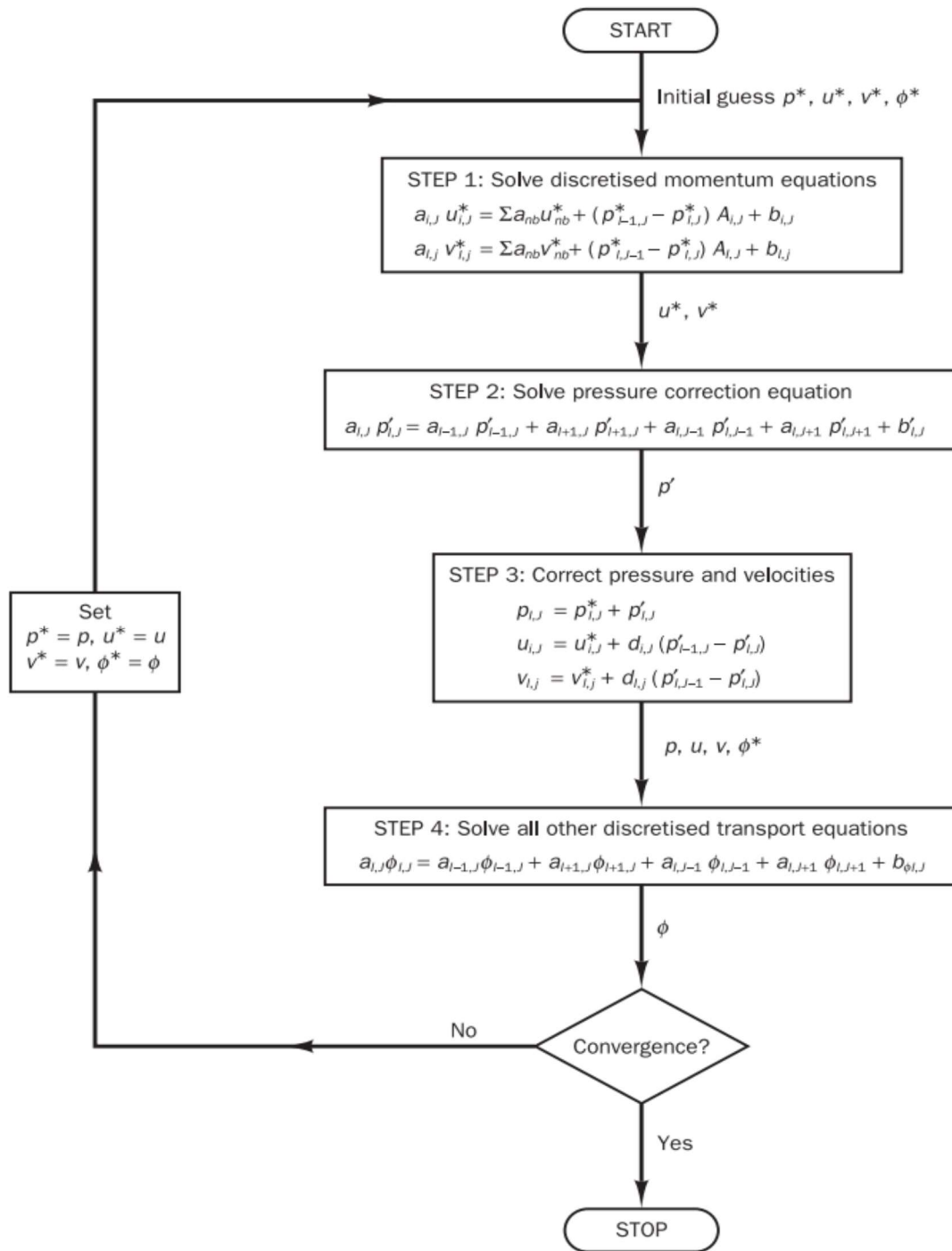


Figure 10: Computational sequence of SIMPLE algorithm (Versteeg & Malalasekera, 2007)

The initial guessed value were assumed and set manually during initialization of the solution. Each iteration go from step 1 to 4, convergence criteria for residual of each equation is set in monitor.

2.10.3. Turbulence models

To make the most appropriate choice of model for our application, we need to understand the capabilities and limitations of the various options. According to the study made by Nielsen the selection of turbulence model is a compromise due to the capability of handling all flow elements in an optimal and economical way (Peter Vilhelm Nielsen, 1988). The choice of turbulence model will depend on considerations such as the physics encompassed in the flow, the established practice for a specific class of problem, the level of accuracy required, the available computational resources, and the amount of time available for the simulation. The turbulent models implemented in STAR CCM+ software are categorized in to two: The Reynolds Average Navier-Stokes equation and Scale-resolving simulation that solve the large scales of turbulence and models small- scale motions. These are Large Eddy Simulation (LES and Detached Eddy Simulation (DES) (STARCCM+, 2017). It has been gone through different literatures in order to select an appropriate turbulent model for this study and it was made a comparison of the different turbulent models. In the following sections it is discussed in detail about the different turbulence models.

2.10.4. K-Epsilon Turbulence

The K-Epsilon turbulence model is a two-equation model that solves transport equations for the turbulence kinetic energy (k) and the turbulence dissipation rate (ϵ) in order to determine the turbulence eddy viscosity (μ_t). A K-Epsilon turbulent model can be applied for a fully turbulent flow but it is appropriate to use for a buoyant flow and it was evaluated numerically stable with correct precision in the results (Catalina, Virgone, & Kuznik, 2009). K- ϵ turbulence model is the most widely used model because of its applicability to wide – ranging flow problems and its lower computational demand than more complex models that are available.

The standard k- ϵ model uses the following transport equation for Turbulence kinetic energy k and Turbulence rate of dissipation ϵ :(Versteeg & Malalasekera, 2007)

$$\frac{\partial(\rho k)}{\partial t} + \text{div}(\rho k U) = \text{div} \left[\frac{\mu_t}{\sigma_k} \text{grad } k \right] + 2\mu_i S_{ij} \cdot S_{ij} - \rho \epsilon \quad 21$$

$$\frac{\partial(\rho \epsilon)}{\partial t} + \text{div}(\rho \epsilon U) = \text{div} \left[\frac{\mu_t}{\sigma_\epsilon} \text{grad } \epsilon \right] + C_{1\epsilon} \frac{\epsilon}{k} 2\mu_i S_{ij} \cdot S_{ij} - C_{2\epsilon} \rho \frac{\epsilon^2}{k} \quad 22$$

2.10.5. K-Omega turbulent model

The K-Omega turbulence model is a two-equation model that solves transport equations for the turbulent kinetic energy k and the specific turbulent dissipation rate ω the dissipation rate per unit turbulent kinetic energy $\left(\frac{\omega}{k}\right)$ in order to determine the turbulent eddy viscosity which is given by $\mu_t = \frac{\rho k}{\omega}$ (STARCCM+, 2017). The biggest advantage of this approach is that ω is known in viscous sublayer.

The transport equation for k and ω for turbulent flow at higher Reynolds is given as follows:

$$\frac{\partial(\rho k)}{\partial t} + \text{div}(\rho k U) = \text{div} \left[\left(\mu + \frac{\mu_t}{\sigma_k} \right) \text{grad}(k) \right] + P_k - \beta^* \rho k \omega \quad 23$$

Where $\varepsilon = \beta^* k \omega$

$$P_k = \left(2\mu_t S_{ij} - \frac{2}{3} \rho k \frac{\partial U_i}{\partial x_j} \delta_{ij} \right) \quad 24$$

Is the rate of production of turbulent kinetic energy and

$$\frac{\partial(\rho \omega)}{\partial t} + \text{div}(\rho \omega U) = \text{div} \left[\left(\mu + \frac{\mu_t}{\sigma_\omega} \right) \text{grad}(\omega) \right] + \gamma_1 \left(2\rho S_{ij} \cdot S_{ij} - \frac{2}{3} \rho \omega \frac{\partial U_i}{\partial x_j} \delta_{ij} \right) - \beta_1 \rho \omega^2 \quad 25$$

2.11. Discretization method

Discretization schemes plays a key factor in the quality of the solution of the flow equations. The type of discretization deals with how governing equations are discretized. The steps involved in discretization of differential equations into a none overlapping control volumes called mesh. Each mesh point in the algebraic equation for the flow variables to be solved by using iterative procedure.

3. Methodology

This chapter discusses the methodologies used for CFD study of an office cubicle designed as per the Norwegian passive house standard. Since Oslo Metropolitan University acquires the license for STAR CCM+ from Siemens CD-adapco, 2016, this software is employed for this study. STAR CCM+ was used to model the office cubicle, and validate the existing experimental results. The software was also used to assess the different turbulence models ability to predict the temperature distribution and air flow pattern in turbulent flow.

Once the geometrical model was developed in STAR CCM+, it discretized into discrete mesh domain. Then physics model and appropriate boundary conditions is implemented in accordance to the existing experimental data. The transmission heat losses through the building elements towards the outdoor environment was calculated by considering the overall heat transfer coefficient of the external wall/window and the temperature difference between the indoor and outer environmental.

3.1. Geometry

The room model was developed based on the existing data as shown in the table 4 (Axel, MYSEN, & THUNSHELLE, 2015). Dimension of the room is 4.25 m length, 2.25 m width and 2.7 m height. The room is designed to accommodate one person and ventilated by mixing ventilation. The human simulator was simplified as a cylinder having a diameter of 0.4 m and height of 1.1 m, an office table with a PC, one Lindvent ceiling mounted air supply diffuser at the center of the ceiling. Room air is extracted with exhaust diffuser having the same dimension of the supply diffuser. Schematic diagram of the room showing the detail of the interior elements is shown in figure 11.

Table 3: Description of the geometry with dimensions and position.

Description	Dimension (m)	Location (m)
Cubicle	4.25 m x 2.25 m x 2.7 m 1.7 m x 2.5 m window	
Manikin (cylinder)	0.4 m diameter by 1.1m height	0.8 m from the window and 0.6 m from the table
Table	2.0 m x 0.8 m at a height of 0.8 m	0.1 m from the window
PC	0.3 m x 0.3 m x 0.4 m	At the center of the table
Inlet diffuser	Diameter of 400 mm and opening hight 35 mm	At the center of the ceiling
Light fixtures	Length 0.15 m and width of 0.7 m	L1 0.68 m from the left wall and 0.42 m from the front wall, L2 1,01m from L1 and 0.42 from the front wall
Outlet duct	Diameter of 250 mm	0.65m from the right and the rear wall and 1.75m from the left wall
Heating element	Length 1m and width 0.2 m	0.45m above the floor and 0.2 m under the window

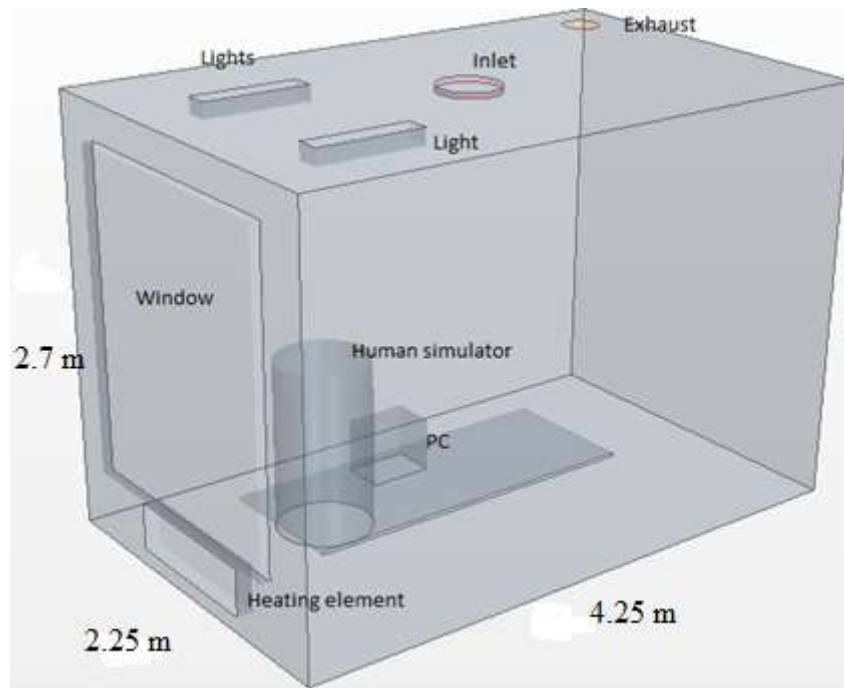


Figure 11. Schematic showing the dimensions, locations of an air supply diffuser, an exhaust diffuser, lights, a human simulator, a pc, and a heating element.

An active diffuser from Lindvet type TTC-250 have diameter 400 mm, opening height 35 mm with six moving slots over a vertical guide (detail geometric description from the product catalogue was shown in the appendix 1).

The active diffuser geometry was simplified as a homogeneous surface in order to reduce computational and meshing complexity. The slots thickness during the simplification was approximated to 1.5 mm. In this case, the new opening height of the diffuser became 26 mm. The geometry for perforated and an open type diffuser was also developed for comparing the effects of diffuser types on the temperature and velocity distribution. The dimensions for the perforated diffuser has 400 mm the diameter, 264 holes with 5 mm diameter each.

3.2. Mesh generation

In this study the computational domain represents the flow field inside the cubicle office which is called a region. The simulation will attempt to predict the fluid flow variables at each and every distinct volumetric cell in the domain by solving the governing equations, which will then be used to validate the turbulence models against the corresponding fluid properties measured experimentally. Meshing process in STAR CCM+: specify mesh models that will be used in continua, assign mesh values, define mesh properties and customize mesh sizes. Once the mesh properties are defined surface mesh is generated then generate volume mesh. An aother alternative for mesh generation is part based meshing. In this case several operations can be set up that alter the geometry, create contacts and perform the actual mesh. The advantage with this approach is that a change can easily be made all the way back to a CAD-level and all changes added with operations updated with the push of a button.

Polyhedral mesh was used in this study as it can provide a balanced solution for complex mesh generation problems, and it is relatively easy and efficient to build, requiring no more surface preparation than the equivalent tetrahedral mesh. Moreover polyhydral mesh contains approximately four times fewer cells than a tetrahedral mesh for a given starting surface (STARCCM+, 2017).

In order to reduce discretization error mesh (grid) independent analysis is implemented. Therefore three different sizes of meshes are generated with the cell sizes of 134714, 194842 and 350814 cells. In grid refinement process, the cells in the region of high air flow and temperature region were mainly increased with the following spacing: 0.05, 0.02, and 0.01 for the heat sources, an exhaust diffuser and the inlet diffuser respectively (see figure 12).

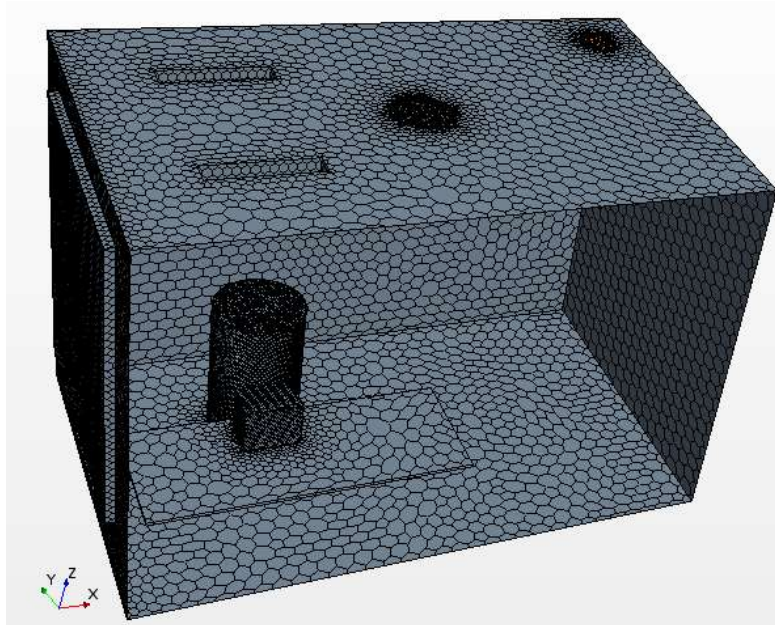


Figure 12: Visual illustration of mesh domain with fine mesh near the inlet, outlet, human simulator and PC

The procedures implemented in generating automated meshmesh and mesh refinement is illustrated in figure 13. Table 4 summarizes the mesh sizes at the supply diffuser and exhaust mesh for the fine mesh.

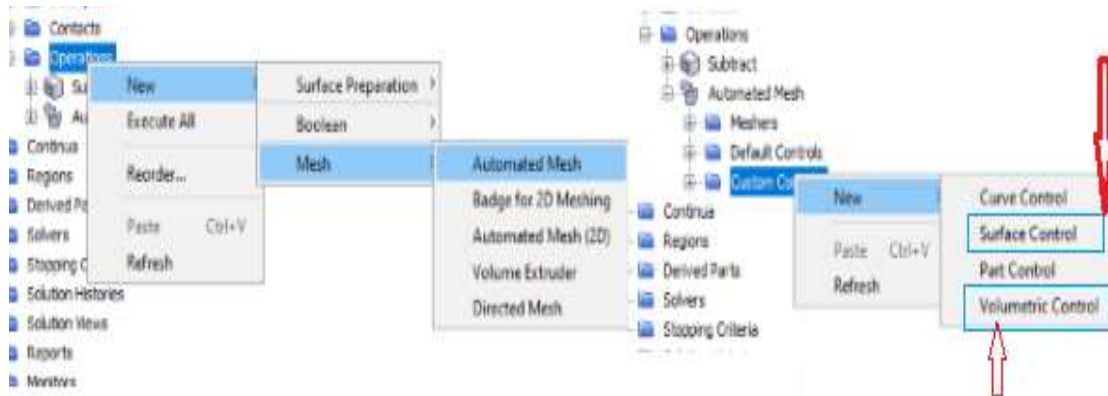


Figure 13: Procedure in generating automated mesh, volume control and surface control

Table 4: Parameter values for supply diffuser and exhaust diffusers employed for mesh refining during automated meshing

Parameters	Surface mesh	Volume mesh
	Exhaust diffuser	Supply diffuser
Base size	0.1 m	0.1 m
CAD Project	Enabled	Enabled
Target surface size	0.02 m	
Minimum surface size	0.01 m	
Number of prism layer	5	7
Prism layer thickness	0.025	0.025
Custom size		0.01 m

3.3. Physics and simulation models

The physics model makes up the governing momentum, energy and turbulent equations to be solved over the computational domain. The physics models in STAR CCM+ code contains many models, in which individual models are brought together to simulate a given physical problem. The flow is assumed to be incompressible as it has sufficiently small velocity. Moreover, the following physics model were included in the simulation: three dimensional, ideal gas, gradients, gravity, steady, segregated flow, segregate flow temperature, turbulent, radiation, grey thermal radiation, surface to surface radiation, Reynolds-average Navier-Stokes and the turbulence models. The segregated flow model solves the equation for the velocity and pressure in a coupled manner, linking continuity and momentum transport equations by means of the SIMPLE algorithm. (STARCCM+, 2017). The remaining physics models are chosen to model the buoyant, turbulent flow and heat transfer for this study. K- epsilon model and K- omega models were compared and Bossinesqu modell was employed in simulations. The models selected for this study are shown in the following figure 14.

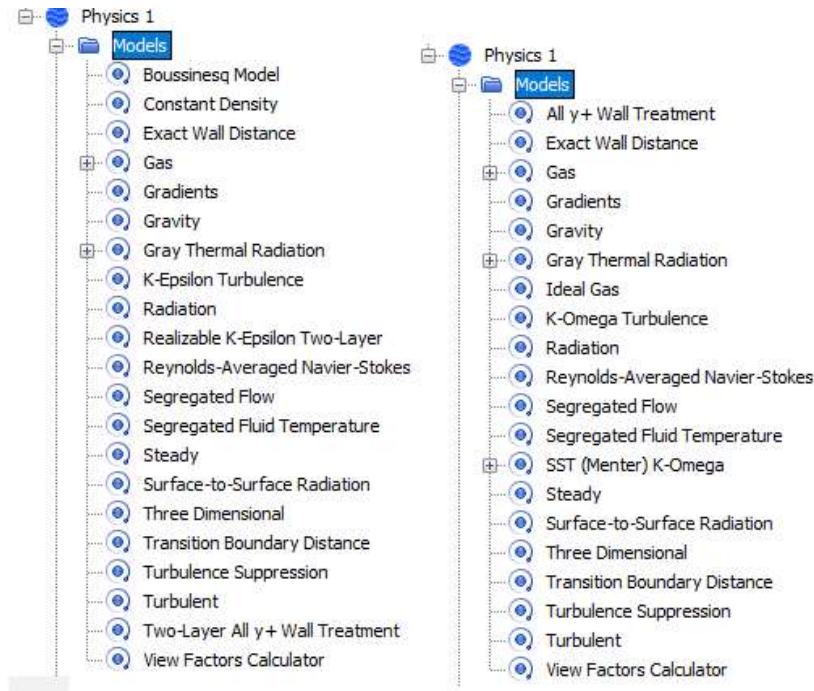


Figure 14: Physics models selected for the simulation

3.3.1. Reynolds-Average Navier-Stokes

In order to simulate turbulent fluid motions, Reynolds decomposes the flow quantities into its average and fluctuating components. The new quantities were substituted to the Navier-Stokes equations and as a result Reynolds Averaged Equations (RANS) were obtained. RANS turbulence models provide closure relations for the Reynolds-Averaged Navier-Stokes equations that govern the transport of the mean flow quantities (STARCCM+, 2017). Components in the transport equations are unknown and cause system of the equation not to be closed. Additional equations which helps us to solve this terms is turbulence model.

To obtain the Reynolds-Averaged Navier-Stokes equations, each solution variable ϕ in the instantaneous Navier-Stokes equations is decomposed into its mean, or averaged value $\bar{\phi}$ and its fluctuating component ϕ' :

$$\phi = \bar{\phi} + \phi' \quad 26$$

Where ϕ represents velocity component, pressure, energy and species concentration can be written as:

$$v_i = \bar{v}_i + v'_i \quad 27$$

$$p = \bar{p} + p'$$

In STAR CCM+ software there are two general approaches to solve the Reynolds stress tensor and there by provide closure to the governing equations: Reynolds stress transport and eddy viscosity (STARCCM+, 2017). The Reynolds stress transport approach is also called the second-momentum closure, it directly solves a transport equation for each component of Reynolds stress tensor. On the other hand the eddy viscosity approach uses the concept of turbulent viscosity (μ_t) to model the Reynolds stress tensor as a function of the mean flow quantities; the function used in STAR CCM+ is Boussinesq approximation.

$$T_t = 2\mu_t S - \frac{2}{3}(\mu_t \nabla \cdot v + \rho k)I \quad 28$$

Boussinesq relationship can be written as $R_{ij} = \overline{-u'_i u'_j} = 2 \frac{\mu_t}{\rho} S_{ij}$

where $S_{ij} = \frac{1}{2} \left(\frac{\partial U_i}{\partial x_j} + \frac{\partial U_j}{\partial x_i} \right)$

Where S it the mean strain rate tensor, v is the mean velocity and I is the identity tensor or the tensor of unity, ρ density and k is the turbulent kinetic energy

$$S = \frac{1}{2}(\nabla V + \nabla V^T) \quad 29$$

$$k = \frac{1}{2}(\overline{u'^2} + \overline{v'^2} + \overline{w'^2}) \quad 30$$

3.3.2. Relaxation

In the iteration process the convergence behavior of the solution can be controlled by means of under-relaxation parameters. The under-relaxation factor is user defined parameter specified between 0 and 1 and it is defined as the degree in which the previous solution results are replaced by the newly determined results (STARCCM+, 2017). In these simulations the parameters for velocity, pressure, k- ϵ turbulence and k- ϵ turbulence viscosity could be adjusted.

3.4. Boundary conditions

The boundary condition tells the CFD solver how the computational domain interacts with its environment. In this study it is specified one region in the room model. As shown in the figure 10 the region is composed of six bounding surfaces of the room, a human simulator model (heat source), PC, heating element (used when it is necessary), two ceiling mounted light fixtures with a capacity of 68W and ceiling mounted an active supply diffused from Lindvent with model KTH 160 B and air return duct with the same diameter as the supply air diffuser was used for this study. Each boundary have its own properties for physics condition and physics values. The data which was used for boundary conditions in the CFD simulation for this study in each physics conditions and values are obtained from the existing experimental data.

The velocity inlet boundary represents a region allowing fluid mass and momentum to enter the computational domain. To solve the set of governing equations, a constant air temperature and constant air flow velocity was considered. The air flow velocity was calculated based on the area of the supply diffuser. The inlet boundary condition was assumed as a uniform velocity (\bar{u}) (m/s), which will be calculated based on the existing data using the following equation.

$$\bar{U} = \frac{Q}{A_i} n \frac{V}{A_i} \quad 31$$

Where Q is the inlet flow rate (m^3/s), A_i the inlet opening area (m^2), n is the number of test room air exchanges (s^{-1}), V is the volume of the room model (m^3).

The inlet flow rates used in the simulation are assumed based on the experimental data, the flow rate at maximum opening based on the operating pressure of Lindvent diffuser and maximum and minimum air volume demanded for a single office with an occupant. For this study, it was imposed a set of inlet velocities considering different flow conditions: 1.5 m/s, 1.07 m/s, 0.65 m/s and 0.43 m/s. The outlet diffuser was considered as a pressure outlet with constant pressure equal to zero gage pressure. The human simulator, PC and lights were considered as a heat sources. The boundary walls around surfaces enclosing the room were considered as adiabatic with no-slip condition, which indicates that the first fluid layer adjacent to the wall sticks to the wall and moves with the same velocity as the wall.

Heat losses from the window and the surface of the facade was included in the simulation and it was assumed that heat flux which was evenly distributed on the façade/window surfaces (RISBERG, WESTERLUND, & I. HELLSTRÖM). The thermal boundaries assumption were described in STAR CCM+ as a environment (calculates the heat loses due to both convection with the environment and conduction through the façade/window) based on the overall heat transfer coefficient of the envelop. The U-values for the externa wall and window was assumed

as 0.14 W/m^2 , and 0.78 W/m^2 respectively (Axel et al., 2015). Figure 15 shows the schematic of boundary condition employed for the office cubicle.

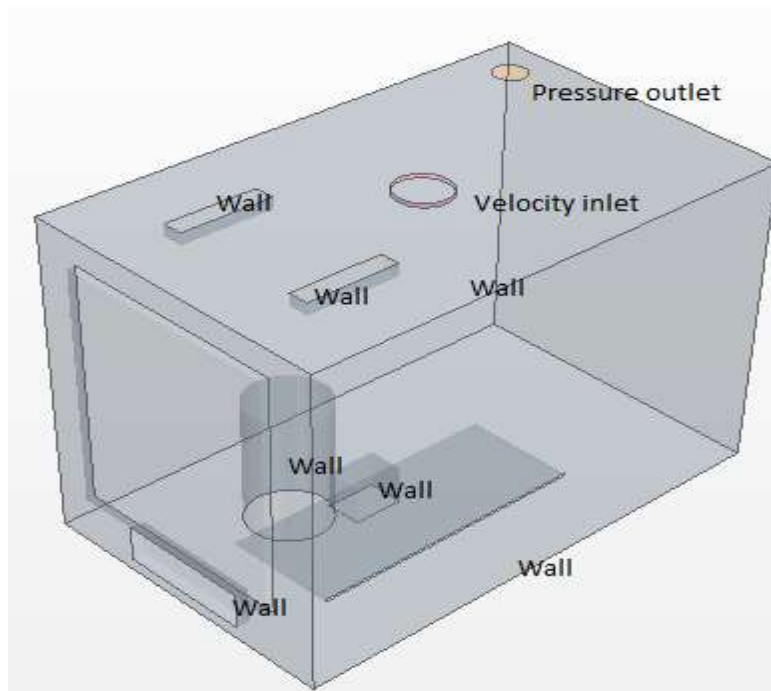


Figure 15: Schematic showing the boundary conditions employed

In the model it is specified thermal boundary conditions by taking into account both convection and radiation, as radiation is the key form of heat release for the heat sources. The outdoor air temperature condition used for the CFD simulation varied between -1.8 and -10 °C for parametric analysis.

The heat sources in the room are consists of one person working on his computer and two lights. The heat generated from the human simulator was assumed as 120 W according to the existing data. The computer and the two lights generate 30 W and 136 W respectively. Table 5 summarizes the details for the boundary conditions employed in this study.

Table 5: Boundary conditions used for CFD model of the cubicle office

Boundary	Type	Mass and momentum	Temperature [°C]	Heat Flux [W/m ²]	Heat source [W]	Turbulence intensity [%]
Velocity inlet	Inlet	V _x = 1.5 m/s V _x = 0.65 m/s V _x = 0.43 m/s V _x = 1.07 m/s	24, 26,28, 30			4
Outlet	Pressure outlet		19			1
Front wall	wall	No-slip wall		adiabatic	-	
Rear wall	Wall	No-slip wall		adiabatic		
Right wall	Wall	No-slip wall		adiabatic		
Ceiling	Wall	No-slip wall		adiabatic		
Floor	Wall	No-slip wall		adiabatic		
Left wall	Wall	No-slip wall		-24.28		
Window	wall	No-slip wall		-24.3		
Lights (1&2)	Wall	No-slip wall			+136	
pc	Wall	No-slip wall			+30	
Table	wall	No-slip wall		adiabatic		
Human simulator	Wall	No-slip wall			+120	
Heating Element	Wall	No-slip wall		adiabatic		

The air flow and temperature measurements were recorded from the simulation result at four different positions with a vertical probe lines P1 located between the table and the human simulator at $x = 1$ m and $y = 1.5$ m, P2 located between the human simulator and the window at $x = 0.6$ m and $y = 1.9$ m, P3 located back the human simulator at $x = 1$ m and $y = 2$ m and P4 located to the right side of the human simulator at $x = 1.6$ m and $y = 1.5$ m.

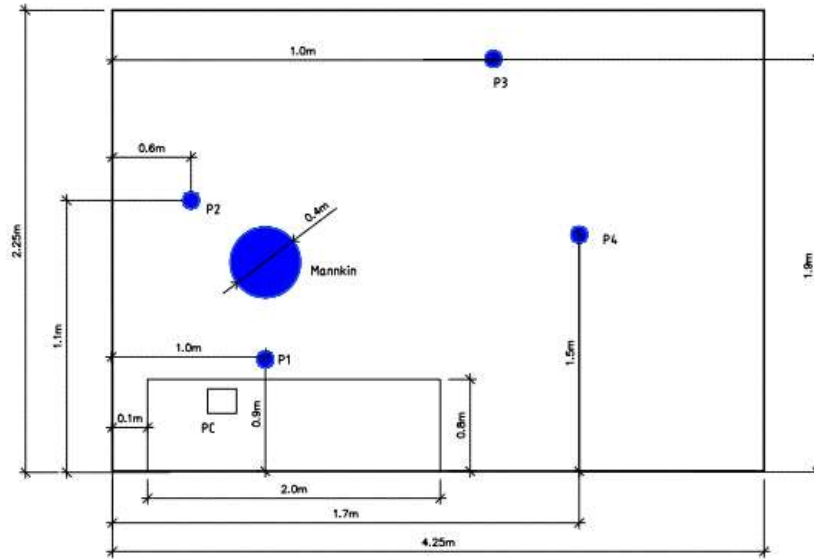


Figure 16: Room configuration and measuring probes layout (P1, P2, P3 & P4) measuring poles and PC and human simulator

3.5. Convergence criteria

Convergence is the point at which the solution no longer changes with successive iterations (Vampati). Convergence criteria, along with the decreasing residual helps in determining the completion of the solution point which is defined by the user. Residuals are a small imbalance that are created during the course of iterative solution algorithm.

In CFD simulation the residual measures the local imbalance of the conserved variables in each control volume. Residual represent the degree to which the discretized governing equations are satisfied collectively by each cell in the discretized mesh. The STAR-CCM+ simulations in this study monitor residuals at every iteration for continuity, energy, X, Y and Z momentum and for the turbulence transport equations. In iterating the numerical solutions, the residual will never be exactly zero, however the lower the residual value is, the more accurate the numerical solution is. For STAR CCM+, when the residual levels reaches minimum below 10^{-3} convergence would be obtained. Therefore, the convergence criteria for this study is set to be below 10^{-3} for continuity, energy, X, Y and Z momentum and for the turbulence transport equations. CFD solution with sufficiently small residual values will lead to small solution imbalances (Mike Kuron, 2015). Another method to check convergence is to monitor whether the values of domain of interest reaches a steady solution and the domain imbalance is less than 1% . Figure 17 shows the residual for the simulation result which are: continuity 10^{-5} , energy 10^{-4} and X,Y,Z momentum, Tdr, Tke, 10^{-7} , 10^{-7} , 10^{-7} , 10^{-8} and 10^{-7} respectively.

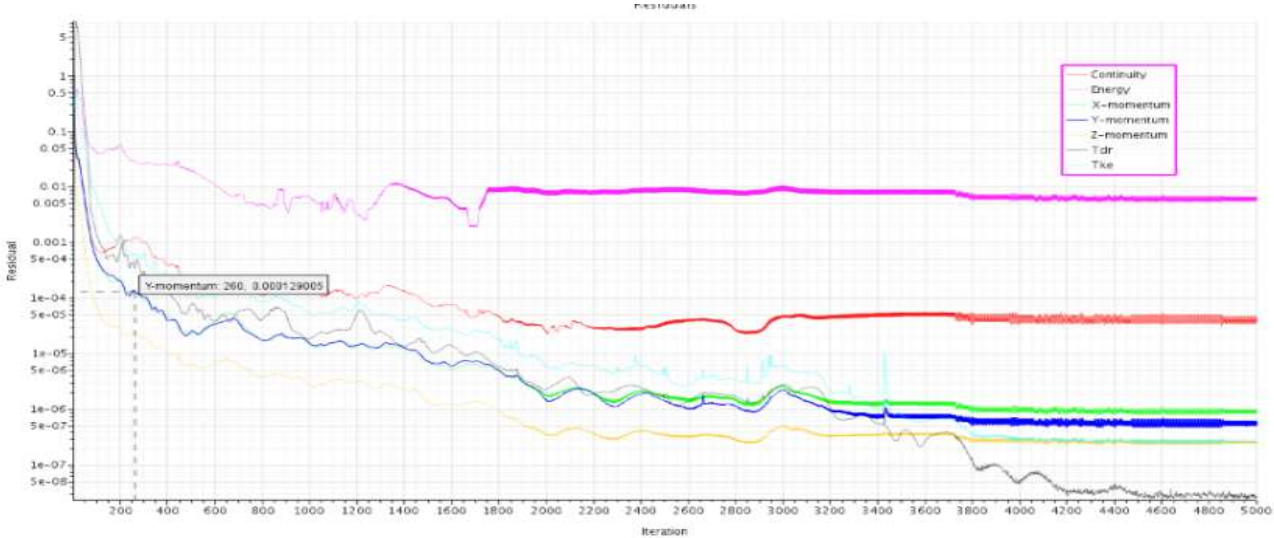


Figure 17: Converged residual for flow rate 177 m³/h simulation

4. Results and discussions

In this study a total of ten cases with 30 simulations have been considered in order to study the effects of supply air temperature and volumetric air flow rates. For most of the simulations convergence was achieved after 5000 iterations. The results for air temperature and air velocity profiles obtained for different meshes and turbulence models are presented in the form of graphs, tables and plots on section planes. For validation purpose results of the simulations are compared with the existing experimental data in Axel et al (Axel et al., 2015). Sensitivity analysis has also been carried out for reference cases by varying one parameter at a time and evaluated the impact of the variable on the simulation result. The detailed configuration conditions for selected simulation cases are given in table 6.

Table 6: Selected cases for numerical simulation

Cases	Volumetric flow rate [m ³ /h]	Supply temperature [°C]	External temperature [°C]	Supply velocity [m/s]	Purpose of simulation
1	177	24	-1.8	1.5	For validation purpose
2	126	24, 26, 28	-1.8	1.07	Sensitivity analysis
3	76	24, 26, 28	-1.8	0.65	Sensitivity analysis
4	51	24, 26, 28	-1.8	0.53	Sensitivity analysis
5	126	24, 26, 28, 30	-10	1.07	Sensitivity analysis
6	76	24, 26, 28, 30	-10	0.65	Sensitivity analysis
7	51	24, 26, 28, 30	-10	0.53	Sensitivity analysis
8	51	24		0.53	With radiator
9	177		-1.8	1.5, 9.56 & 0.393	Comparison of two different diffusers
10	177		-1.8	1.5	Grid refinement analysis

4.1. Grid independence analysis

Grid independence analysis is conducted in order to reduce discretization errors and computational time. The three different mesh sizes used to check the model solution convergence are course, 134714; medium, 211301; and fine, 350814. In grid refinement process, the meshes mainly in the region of high air flow and high temperature are increased with spacing: 0.05 m, 0.02 m and 0.01m for the heat sources, outlet diffuser and the inlet

diffuser respectively. The simulation shows the computational times for the mesh sizes of course, medium and fine grids are 1.151 hr, 1.737 hr and 2.62 hr respectively.

Figure 18 shows air temperature and velocity profiles along vertical probe 4. The result shows that the vertical temperature profiles for the three mesh sizes are nearly the same. However, the velocity profile for cell 1 deviates from cell 2 and cell 3 which are virtually identical.

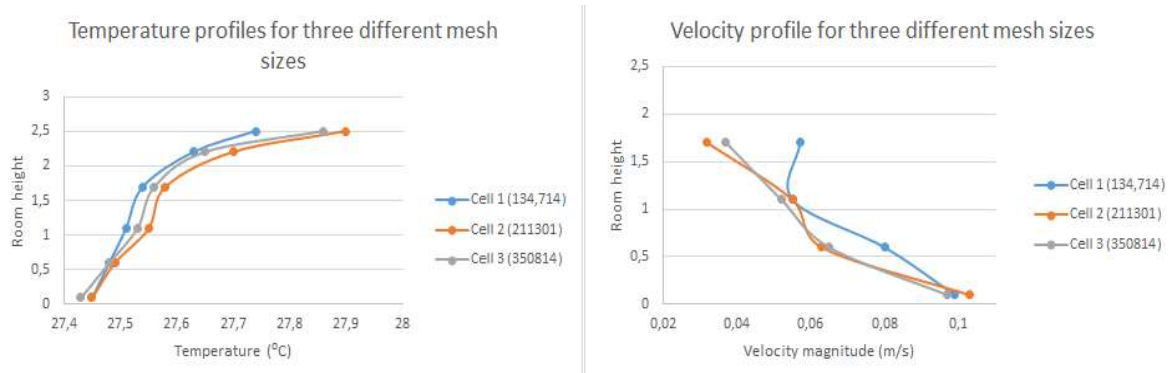


Figure 18: Comparison of temperature and velocity profile for three different mesh sizes: cell 1(134714), cell 2 (211301) and cell 3 (350814).

From grid analysis point of view, it is important to study the effect of mesh size on the mass flow rate and heat transfer rate at the inlet and exhaust of the diffusers (Ning, 2015). This is shown in table 7 for the three different mesh sizes. It is observed that there is negligible difference between cell size 2 and cell size 3, however cell size 1 is slightly different. The following results are based on the finest mesh, cell 3 (350814).

Table 7: Comparison of mass flow rate and heat transfer for three different mesh sizes

	Elements	Cell size 134714	Cell size 211301	Cell size 350814
Mass flow rate (kg/s)	Inlet	-0.05787165	-0.05797162	-0.058005
	Outlet	0,05787163	0.0579161	-0.058059
	Total	-2x10 ⁻⁸	-1x10 ⁻⁸	1.2x10 ⁻⁶
Heat transfer (W)	Inlet	-17249.63	-17279.45	-17289.34
	Outlet	17455.39	17485.35	17492.7
	Total	205.76	205.6	203.36

4.2. Validation of CFD simulation with experimental data

To investigate whether STAR CCM+ can be used to study flow phenomena in office cubicle, it is important to validate the CFD simulation with the available experimental data. For this

purpose the CFD simulation results are compared with the existing experimental data reported by Axel et al (Axel et al., 2015) for the same office cubicle.

Two different turbulence models were chosen for the CFD simulation, and the results are compared with the experimental data as shown in figure 19. Regarding the air temperature profile, no clear difference is observed between the k-ε and k-ω turbulence models. However, the k-ε model reproduces the velocity profile of the experimental data better than k-ω model. Moreover, k-ε model shows a better solution convergence for both momentum and energy (10^{-5} and 10^{-4} respectively). Therefore, k-ε is selected for this study.

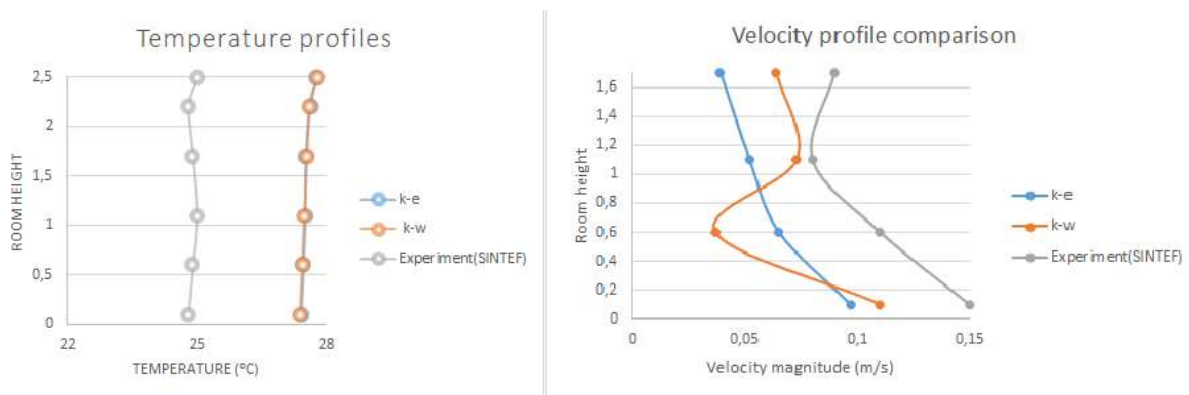


Figure 19: Comparison of simulation results with experimental data reported by Axel et al (Axel et al., 2015) .

Table 8 shows quantitative comparison of vertical temperature gradients for the simulated results and experimental data.

Table 8: Quantitative comparison of temperature distribution between measured and simulated result for Validation

Hight	Expermental data (SINTEF)	Simulation results		Absolut difference K- ϵ	Absolutte difference K- ω model	Error (%) K-w	Error (%) K-e
		K- ϵ Model	K- ω model				
0,1	24.8	27.43	27.41	2.63	2.61	10.6	10,6
0,6	24.9	27.48	27.46	2.58	2.56	10.3	10,4
1,1	25	27.53	27.51	2.53	2.51	10.1	10,1
1,7	24.9	27.56	27.57	2.66	2.67	10.6	10,7
2,2	24.8	27.65	27.62	2.85	2.82	11.5	11,5
2,5	25	27.78	27.82	2.78	2.82	11.1	11,1

The common errors in CFD simulations include discretization error, model error, users related errors (for example: poor geometry and mesh generation, selection of physics models, use of boundary condition) and iteration or convergence error. In addition to the errors in CFD simulation, measurement uncertainty has also impacted in the validation accuracy. The ranges of allowable errors in CFD simulation for validation purpose has been described in different studies. Chen. Q & Srebric Jr (2002) suggested a 20 % error as an allowable for a complex flow problems, whereas Qasim. H, Sabah A & Ala'a. M, (2014) and Ashan.I et al (2013) suggested a 15% error between simulated and experimental results for temperatures and velocity of room air. In table 8, it is shown that the calculated percentage errors for both turbulence models are in the range of (10.1 % – 11.5 %). And velocity errors for both turbulent models are in the range of 0.6 % - 5.3 %. Therefore the results of this study are in good agreement with the experimental data reported by Axel et al (Axel et al., 2015).

4.3. Parametric analysis

4.3.1. Effect of supply air temperatures

To study the effects of supply air temperature, three different cases with different air volumetric flow have been considered. In the first scenario, the volumetric flow rate has been kept at 126 m³/h (case -2 as per table 6), while the supply air temperature varies between 24 °C and 28 °C. In the second and third scenarios, the air volumetric flow rate has been kept at 76 m³/h (case-3) and 51 m³/h (case -4) respectively, while the temperature varies between 24 °C and 28 °C. In all cases, the outdoor temperature is kept at -1.8 °C and -10 °C.

Figures 20-24 present results for temperature and velocity distribution for the different volumetric flow rates and an external air temperature of -1.8 °C. In all cases, varying the supply air temperature produces a thermal plume and cold updraft with stream effects. This is due to the temperature difference between the surfaces of the heat sources (human simulator, PC and lights), the room air. Moreover, the results show air temperature over the heat sources increases with room height, particularly on the left side of the room lead to formation of small temperature gradients.

Figure 22 (a) shows the vertical air temperature profile for the flow rate of 126 m³/h at the supply air temperatures of 24 °C, 26 °C and 28 °C. The result shows no significant vertical temperature gradient, which indicates that there is relatively good air mixing with a temperature effectiveness of 0.93 as calculated based on equation (4). The calculated Archimedes number show a slight reduction from 0.0278 – 0.02614 with an increase in air temperature from 24 °C to 28 °C, this is an indication of the dominance of momentum flow over buoyancy.

Figure 21 shows the velocity contour on a vertical plane A for flow rate of 126 m³/h at different supply temperatures. The radial flow jet of the supply diffuser turned around and fell down after it reaches the edge of the room and entrained the occupied zone. Near the floor and around the heat sources there are many eddies, and this has probably created a good mixing of air as shown in velocity vectors in figure 20. This implies that in the upper level of the room, the flow is affected by the injection of the supply jet. At the lower part of the room, around the heat sources (human simulator & PC), the increase in velocity may be caused by the increase in air temperature along the room height. This may increase the buoyancy force resulting an increase in upward air velocity along the heat sources. As a result the increase in the upward flow velocity along the heat sources causes the temperature gradient increases in the room.

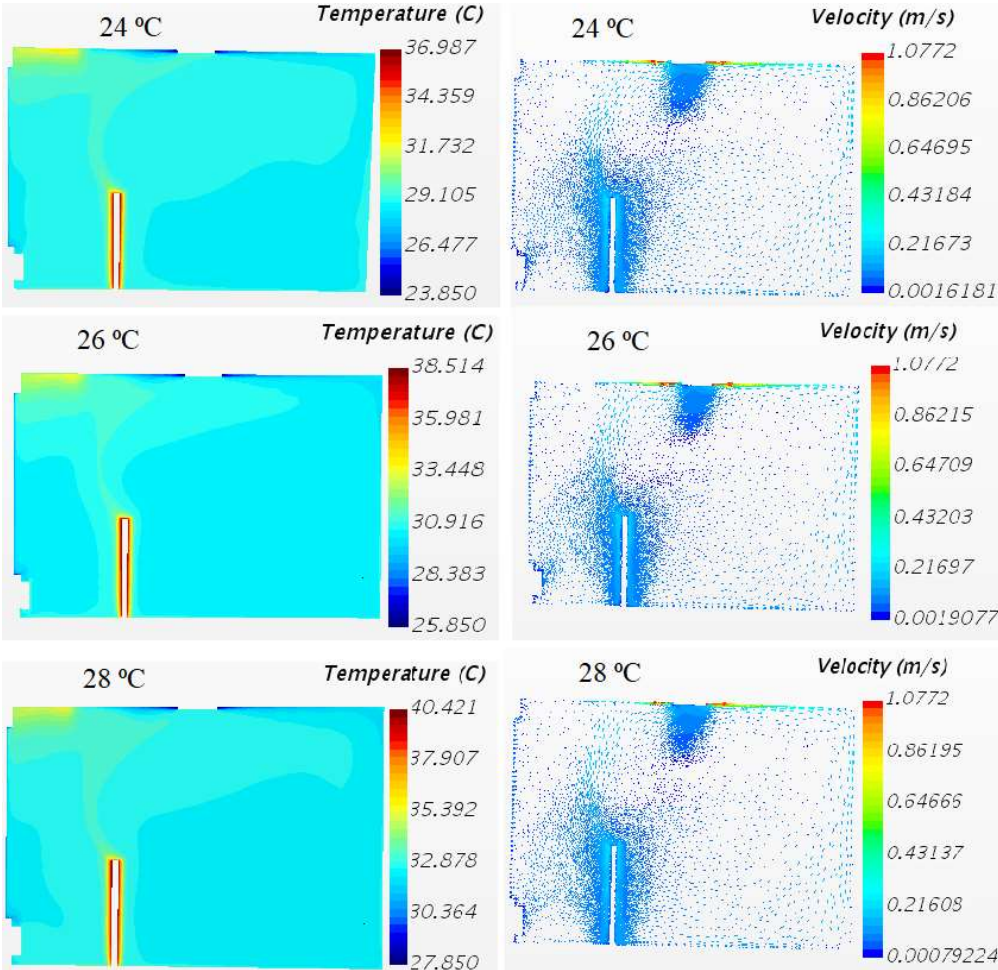
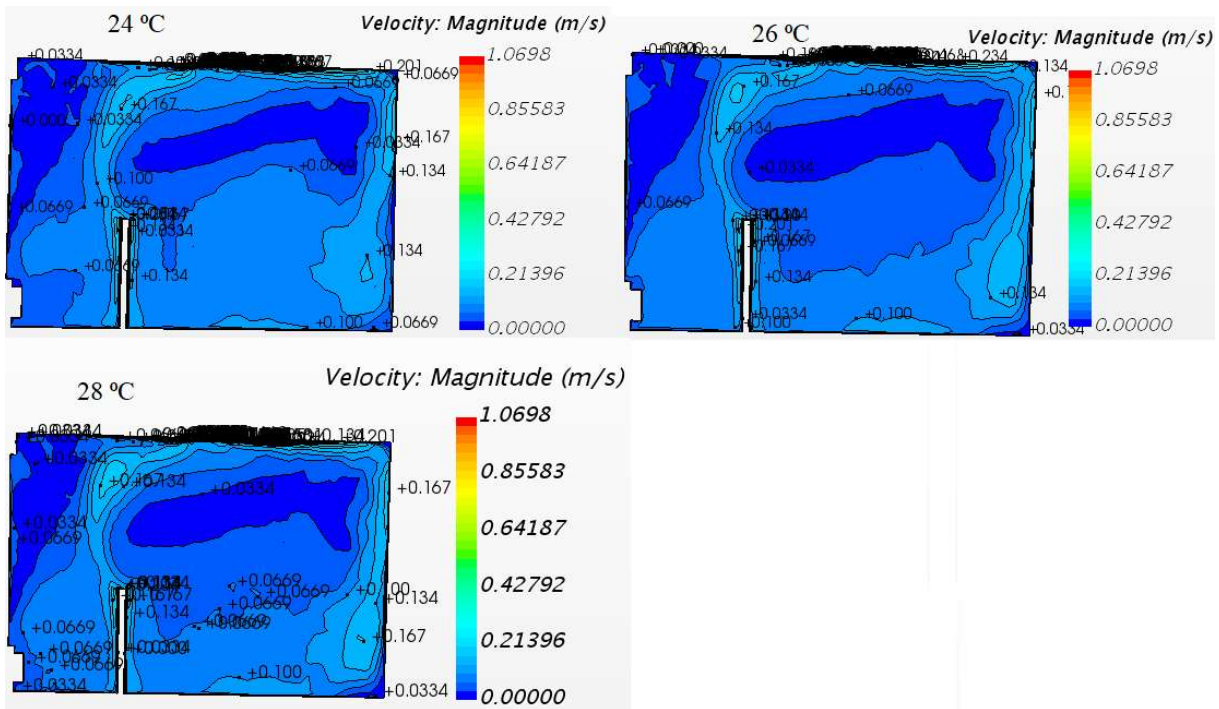


Figure 20: Temperature distribution on plane A & B at different temperatures for case 2 with volumetric flow rate of 126 m³/h for external temperature of -1.8 °C.



The results for flow rate of $76 \text{ m}^3/\text{h}$ shows that the temperature inside the room at the lower right hand side of the heat sources is almost uniform, except for the supply air temperature of $28 \text{ }^\circ\text{C}$ (see figure 23). Whereas the vertical temperature gradient at the upper left part of the room, near the lights, is observed to be higher creating thermal stratification zone near the corner. The calculated Archimedes number, in this case, is within the range $0.1147 - 0.1059$. The result also indicates a better mixing in the room air is achieved at a supply air temperature of $28 \text{ }^\circ\text{C}$ compared with above case and the supply air temperatures of $24 \text{ }^\circ\text{C}$ and $26 \text{ }^\circ\text{C}$ with a temperature effectiveness of 1.02, which is also a good indication for effective room air mixing.

Regarding the velocity contour, the same observation is found for flow rate $126 \text{ m}^3/\text{h}$ (see appendix 3) indicating that the radial flow jet of the supply diffuser turned around and fell down after it reaches the edge of the room. Large eddies are observed near the surface of the the floor at ht right side of the room, over the surface of the heat sources, and at the top of the ceiling near the supply diffuser. This has a clear implication for the occurrence of a good mixing in the room, and thus the flow is affected by the supply jet.

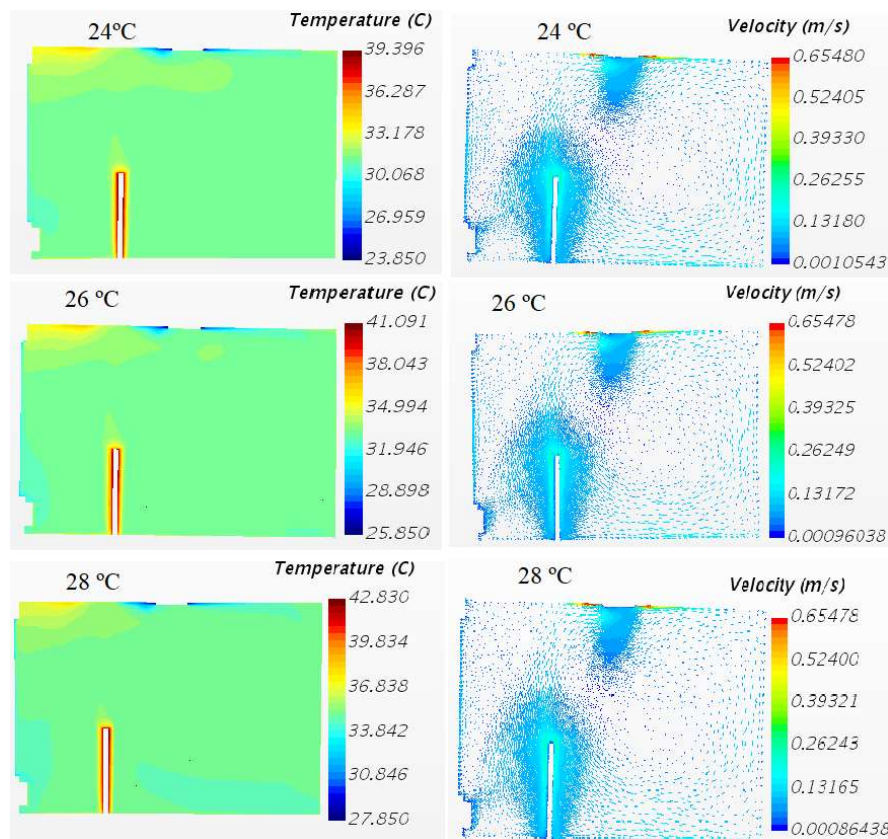


Figure 23: Temperature and velocity distribution on plane A for case 3 at different temperatures with volumetric flow rate $76 \text{ m}^3/\text{h}$ for external temperature of $-1.8 \text{ }^\circ\text{C}$.

For the case when the air supply flow rate of $51 \text{ m}^3/\text{h}$, the room air temperature and velocity distribution results are shown in figure 24. Unlike for the above two cases with air flow rates of $126 \text{ m}^3/\text{h}$ and $76 \text{ m}^3/\text{h}$, the supply jet throw length is very short for all supply air temperatures. The flow from the diffuser falls almost freely down directly to the floor and spread across the floor surface of the room and rises as the air warms due to heat exchange with heat sources in the room. It is also shown that the air temperature distribution along the vertical plane varies creating a clear thermal stratification along the height of the room. After stratification was developed the jet fluid becomes relatively denser at the middle than the surrounding. The colder air reaches the floor surface and spreads more as the supply air temperature increases from $24 \text{ }^\circ\text{C}$ to $28 \text{ }^\circ\text{C}$. This implies that an increase in supply air temperature influences the vertical mean air temperature gradient as shown in table 9. The calculated Archimedes number, in this case, is within the range 0.3433 to 0.3295. The result also reveals that a calculated temperature effectiveness for all supply air temperature is greater than one, which implies that there is an achievement in good ventilation efficiency with respect to temperature effectiveness.

Various observations regarding velocity contour and vectors for flow rates $126 \text{ m}^3/\text{h}$ and $76 \text{ m}^3/\text{h}$ are given in appendix 4 and figure 2. The results show that supply jet falls down to the floor almost freely. This indicates the jet flow for the supply air temperatures of $26 \text{ }^\circ\text{C}$ and $28 \text{ }^\circ\text{C}$ reaches the floor surface and spreads across the floor surface. However, it doesn't cover the whole floor area. This suggests that the supply air jet dominates the thermal plume generated from the heat sources. On the other hand, the flow jet for the supply air temperature of $24 \text{ }^\circ\text{C}$ does not reach the floor. This is due to the fact that the high temperature from the bottom region of the room heats up the supply air and prevents it from penetrating the occupied zone, and from reaching the floor. This implies that the flow is dominated by the upward moving streams of the thermal plume from the heat sources.

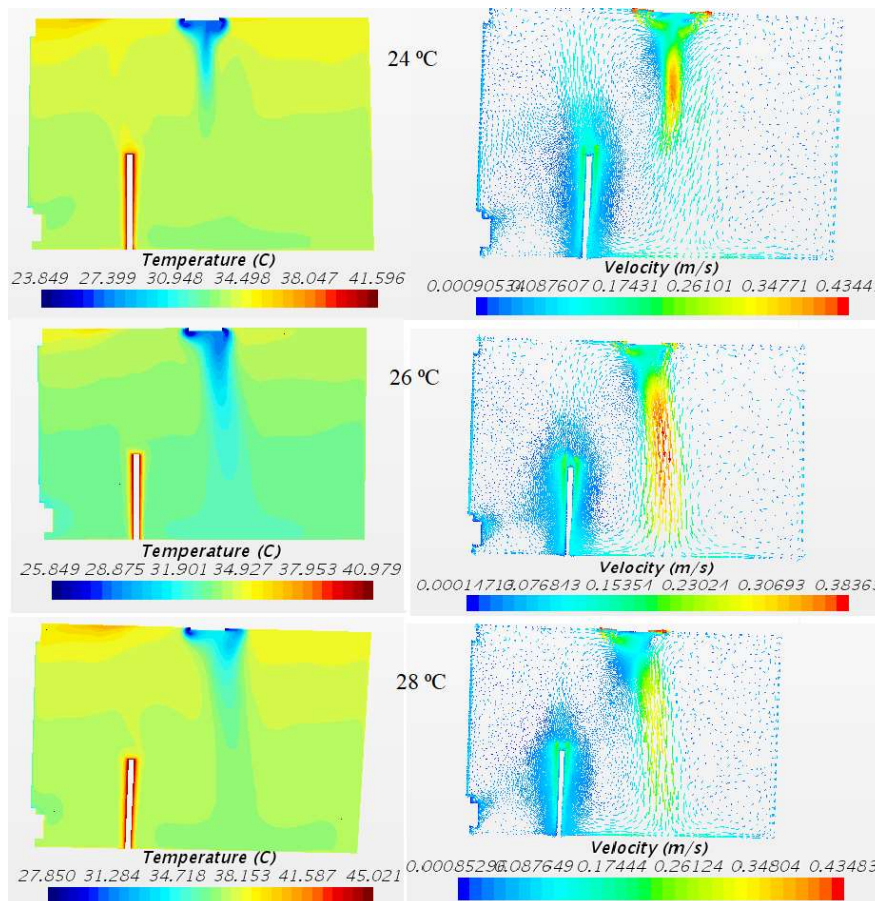


Figure 24: Temperature and velocity distribution for different temperature for flow rate 51 m³/h for external temperature of -1.8 °C.

Table 9: Vertical air temperature difference in occupied zone between 0.1 m and 1.7 m for different supply air temperature and flow rates

Flow Rate (m ³ /h)	Supply air temperature at 24 °C	Supply air temperature at 26 °C	Supply air temperature at 28 °C
126	0.09	0.1	0.07
76	0.05	0.06	0.06
51	0.1	0.7	0.75

Figures 25-27 present results for temperature and velocity distribution for the various volumetric flow rates at an outdoor air temperature of -10 °C. In all cases, varying the supply air temperature produces a thermal plume and cold updraft with stream effects. This is due to the temperature difference between the surfaces of the heat sources (human simulator, PC and lights), the room air and the temperature difference between the outdoor surface of façade/window temperature. Moreover, as highlighted above the results show air temperature

over the heat sources increases with room height, particularly on the left side of the room lead to formation of small temperature gradients.

Figure 25 shows the air temperature distribution for the flow rate of 126 m³/h at the supply air temperatures of 24 °C, 26 °C, 28 °C and 30 °C. The result shows no significant difference on vertical temperature gradient (see appendix 5). This indicates that there is relatively good mixing with a temperature effectiveness of 1.07 and 1 as calculated based on equation (4). The calculated Archimedes number show a slight reduction from 0.0232 – 0.0210 with an increase in air temperature from 24 °C to 26 °C, this is an indication of the dominance of momentum flow over buoyancy. There is no clear difference between the result for supply air temperatures of 28 °C and 30 °C on the air temperature distribution on the right side of the room as shown in the figure 25. However the thermal plum for the supply air temperature of 28 °C dominates the vertical flow over the heat source. In comparison with the previous case the effects of the outdoor temperature of -10 °C has shown no significant difference in the vertical room air temperature gradient for supply air temperature of 24 °C and 26 °C. However there is a slight difference for supply air temperature of 28 °C, this is probably due to the heat loss with the outdoor environment through the façade/window. This implies that the outdoor temperature affects the room air temperature distribution.

Figure 25 and appendix 5 show the velocity vectors and contours respectively. Results show that the radial flow jet of the supply air diffuser turned around and fell down after it reaches the edge of the room and entrained the occupied zone for all supply air temperatures. Many eddies are observed cross the floor at the right side of the room, around the heat sources, on the left side of the heat sources and around the window. This has probably created a good mixing of room air. The velocity contours for supply air temperature 24 °C shows some difference from the rest of the supply air temperatures. The velocity contours and vectors reveals that the flow velocity over the heat source is dominated by the supply jet. On the other hand, the velocity contours and vectors for the remaining supply air temperatures show the flow over the heat sources is generated by the convective heat transfer between the heat sources and the room air and moves upward over the heat sources creating a thermal plum. This implies that the flow in the upper level of the room is affected by the injection of the supply jet, however in the lower part of the room, around the heat sources (human simulator & PC) and the window the increase in velocity is caused by the increase in air temperature along the room height. In addition to this the heat transfer through the façade/window also has contributed its impact on the velocity increase around the window. Therefore, this shows the flow inside the room can be influenced

by the outdoor temperature due to heat loss between the outdoor environment and the façade/window.

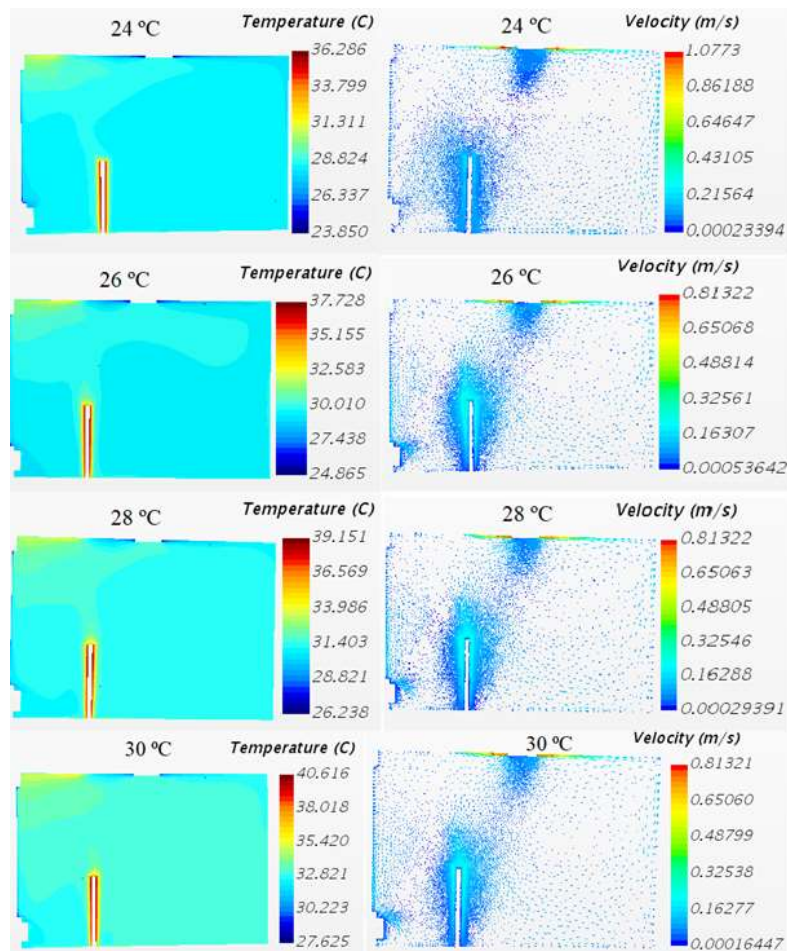


Figure 25: Temperature and velocity distribution for case 5 (126 m³/h) for different temperatures at external temperature (-10 °C)

For flow rate 76 m³/h a high vertical air temperature gradient at a supply air temperature of 24 °C is observed (see appendix 4). The result shows the upward moving thermal plume from the heat source is clearly seen, and there is a clear increase in temperature in the room on both side of the heat source. An observed separation up to the middle on the window side is an indication of the heat transfer between the room air and the outdoor environment. Whereas, for supply air temperature of 26 °C and 28 °C the room air temperature distribution is almost identical with case 3, except a slight domination of the supply jet on the right top part of the room near the ceiling. On the other hand, the air temperature distribution for the supply air temperatures of 28 °C and 30 °C is almost the same, showing a clear separation due to air density differences between top and bottom on both side of the heat sources. This indicates that the room air flow is dominated by the buoyancy of the heat plume from the heat sources.

The same observation regarding the velocity contour and vector is shown in appendix 5 and figure 26 indicating that the radial flow jet of the supply diffuser turned around after it reaches the edge of the room but not falling down to the floor. Then, creates a circulating vortices around the right part of the room which is caused by the stream of the upward moving thermal plume. Large eddies are observed near the surface of the the floor at the right side of the room, over the surface of the heat sources, and at the top of the ceiling near the supply diffuser. This has a clear implication for the occurrence of a good mixing in the room, and thus the flow is mostly driven by the updrift flow of the thermal plume. Comparing case- 3 with case-6 the velocity distribution for the supply temperature 28 °C has no clear difference, and an identical flow velocity distribution is observed with the the supply air temperature of 30 °C. This implies that the outdoor temperature has not affected the air flow velocity inside the room.

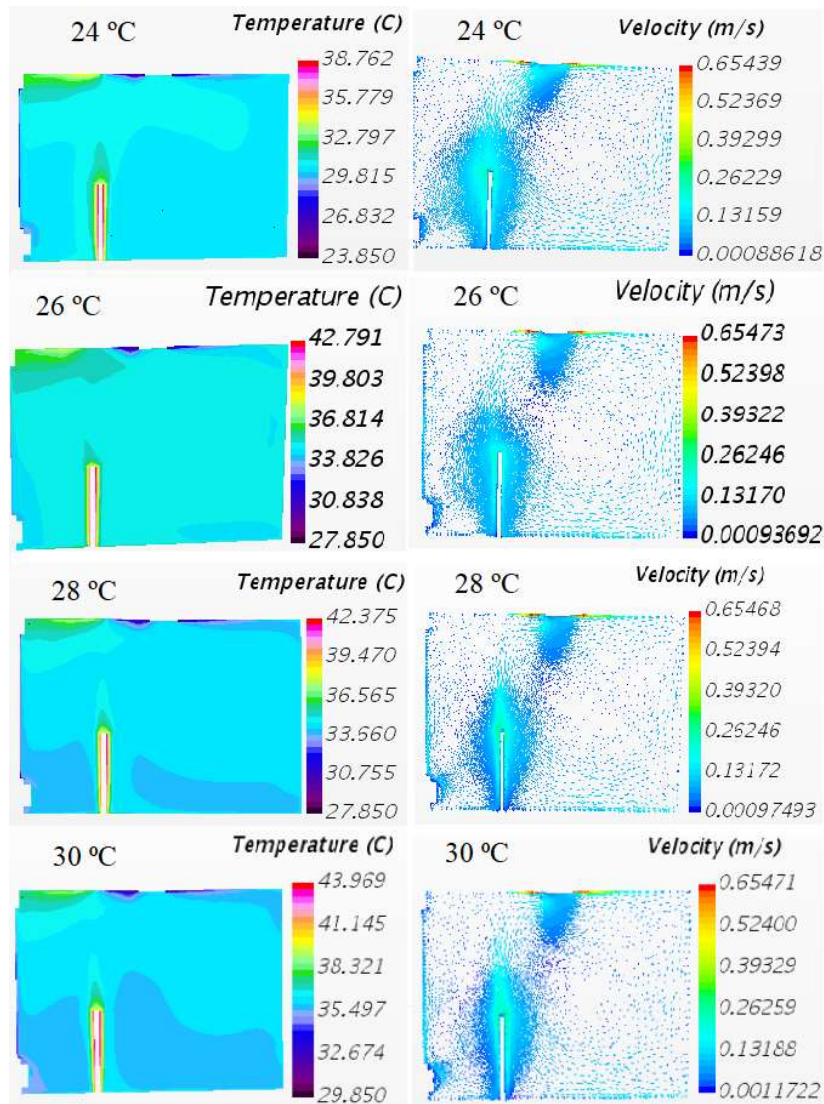


Figure 26: Temperature and velocity distribution for case 6 (76 m³/h) at different temperature external temperature (-10 °C)

For flow rate 51 m³/h for all supply air temperatures the flow is dominated by the upward moving of the thermal plum. Even though most the room air flow is dominated by the upward moving thermal plum, the the supply jet at the upper right part of the heat sources near the exit of the supply diffuser has shown some effect for supply air temperatures 24 °C, 26 °C and 28 °C (see figure 27). Comparing this with the previous case-4 the thermal stratification as well as the vertical temperature gradient has reduced (see appendix 4). This indicates that the outdoor temperature affects the temperature distribution inside the room due to the heat transfer (heat loss) between the façad/window and the external environment.

Figure 27 and appendix 5 show the velocity vectors and contours respectively. Results show that the creation of vortices on the far right side of the room, because of the upward flow of the updraft plum from the heat sources drives the flow. For all supply temperatures 24 °C, 26 °C and 28 °C the same effect is observed. However, for flow rate of 30 m³/h the high velocity at the upper right part of the occupied zone is disappeared. This is indicates that an increase in supply temperature for colder outdoor temperature affects the flow distribution inside the room. For this case the results suggest that an increase in supply temperature from 24 °C to 30 °C with a decrease in volumetric flow rate at an outdoor temperature of -10 °C reduces the thermal stratification. This is due to the heat transfer(loss) between the façade/window and the outdoor ienviroment.

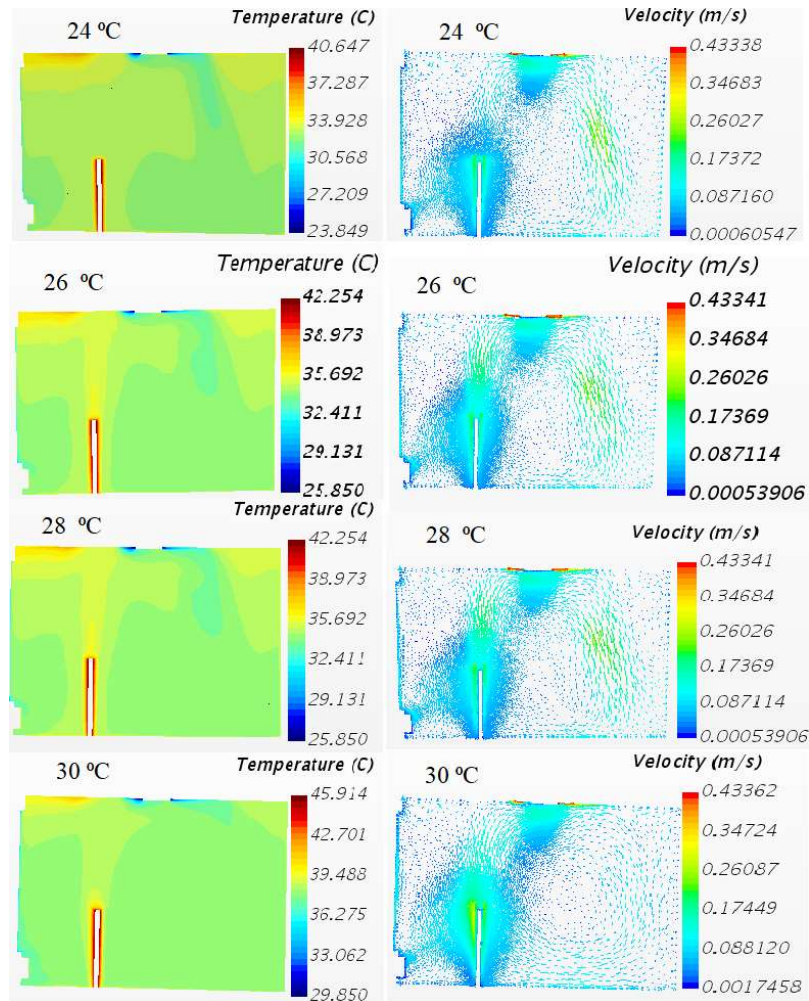


Figure 27: Temperature distribution and velocity vector for case 7 ($51 \text{ m}^3/\text{h}$) for different temperature at external temperature ($-10 \text{ }^\circ\text{C}$)

4.3.2. Effects of volumetric flow rate

In order to study and investigate the effect of low and high supply air flow rate on the performance of the mixing ventilation system, simulations with a volumetric flow rates of $51 \text{ m}^3/\text{h}$, $126 \text{ m}^3/\text{h}$, $76 \text{ m}^3/\text{h}$ and $177 \text{ m}^3/\text{h}$ have been conducted at constant supply air temperature of $24 \text{ }^\circ\text{C}$. In the preceding sections it has been highlighted that the velocity and temperature distribution for the air flow rates of $126 \text{ m}^3/\text{h}$, $76 \text{ m}^3/\text{h}$ and $51 \text{ m}^3/\text{h}$ with a supply air temperature of $24 \text{ }^\circ\text{C}$. The present section includes comparison with flow rate $177 \text{ m}^3/\text{h}$. The results in figures 28 - 30 show investigation of the effects of different volumetric air flow rates ($177 \text{ m}^3/\text{h}$, $126 \text{ m}^3/\text{h}$, $76 \text{ m}^3/\text{h}$ and $51 \text{ m}^3/\text{h}$) with supply air temperature ($24 \text{ }^\circ\text{C}$) along the vertical plane A.

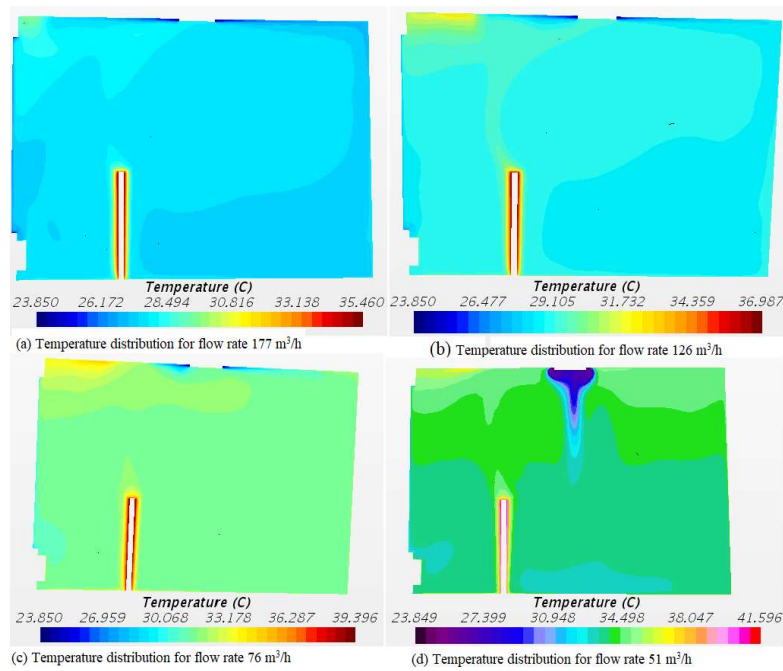


Figure 28: Temperature distribution inside the room for different volumetric flow rates

The contours of air temperature distribution for flow rate 177 m³/h (a) and flow rate 126 m³/h (b) are relatively similar compared to the air temperature distribution for flow rates 76 m³/h (c) and flow rate 51 m³/h (d) but with different magnitude. Air temperature distribution along the vertical plane shows a clear temperature variation for all simulated flow rates along the height of the room. The thermal plume over the heat sources dominates the cold jet from the supply jet flow thus, the room air temperature increases with a decrease in flow rates, this is probably due to decrease in the volume of supply air. The trend for velocity distribution was also almost the same for case 1 and case 2.

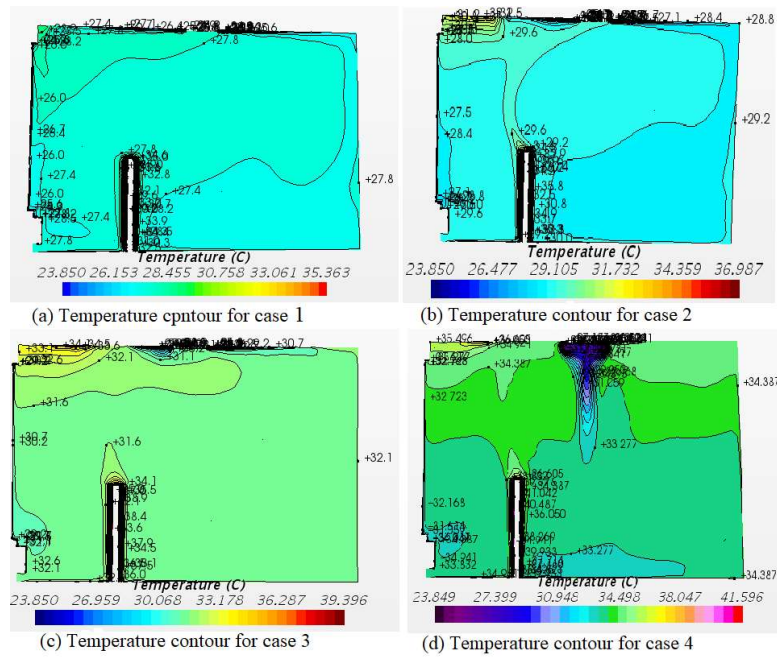


Figure 29: Temperature contour for cases 1 (177 m³/h),2 (126 m³/h),3 (76 m³/h) and 4 (51 m³/h).

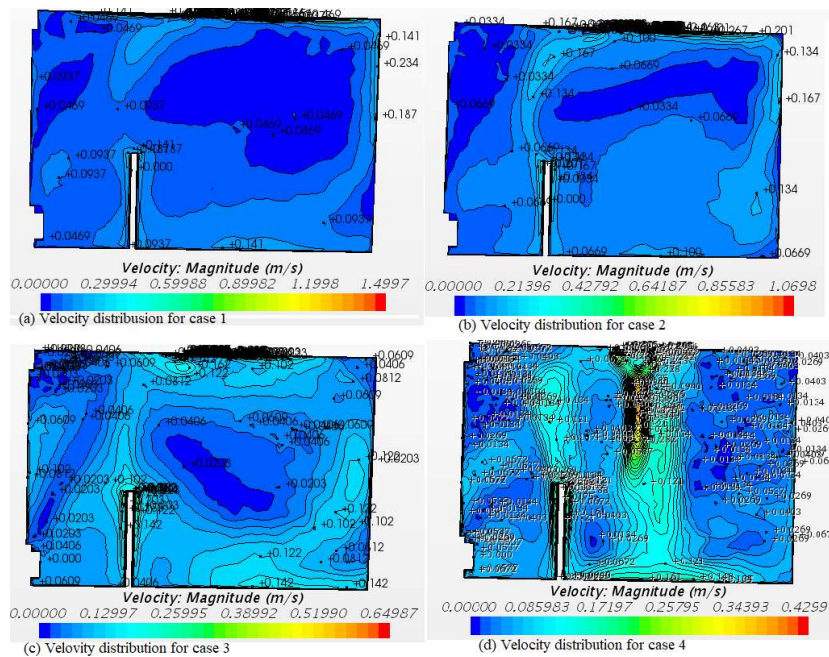


Figure 30: Velocity contours for different volumetric flow rates

Figures 29 and 30 show the contour plots of temperature and velocity flow distribution on a vertical plane A for the four mentioned cases. It has been highlighted in the previous section about the velocity distribution for the flow rates 126 m³/h, 76 m³/h and 51 m³/h, but not for flow rate 177 m³/h. The velocity contour for flow rate 177 m³/h shows the flow velocity inside the room is almost uniform, having the supply jet turning around and reaches the floor over the wall and spread on the floor then, creates a good air mix at the lower level of the room.

Afterwards move over the heat sources. In comparison the result reveals relatively a flow rate $177 \text{ m}^3/\text{h}$ creates uniform flow better than the other three flow rates.

4.3.3. Effect of conventional heating element

The investigation of an effect of additional heating element on the temperature and velocity distribution of the room air has been conducted. From the results in the previous sections the higher thermal stratification occurred at the case when the air flow rate is $51 \text{ m}^3/\text{h}$ and supply air temperature at $26 \text{ }^\circ\text{C}$. This worst case scenario has been selected for this study. The boundary condition for the radiator was assumed as heat source with constant heat flux of (200W). Figure 31 shows the results with and without heating element and at an outdoor temperature of $-1.8 \text{ }^\circ\text{C}$. Velocity vectors in figure 31 (b) & (d) shows the flow velocity generated over the heating element is relatively higher, and hot air moves upward along the window then to the ceiling. Some of the hot air moves downward under the heating element owing to the heat exchange to the near environment.

The result also shows the conventional heating unit influences the airflow inside the room, in such a way that the supplied jet is driven by the density difference of the air at the bottom section, moving over the heat sources. Whereas figure 31 (a) shows the heat from the radiator creates two stratification zones compared to the case with out radiator having four clear stratification zones. The reduction in the stratification zone is due to the buoyancy force effect induced by the heating element. The buoyancy around the heat sources is higher and this is reflected by Archimedis number with values 0.539 for flow region with radiator and 0.298 without radiator.

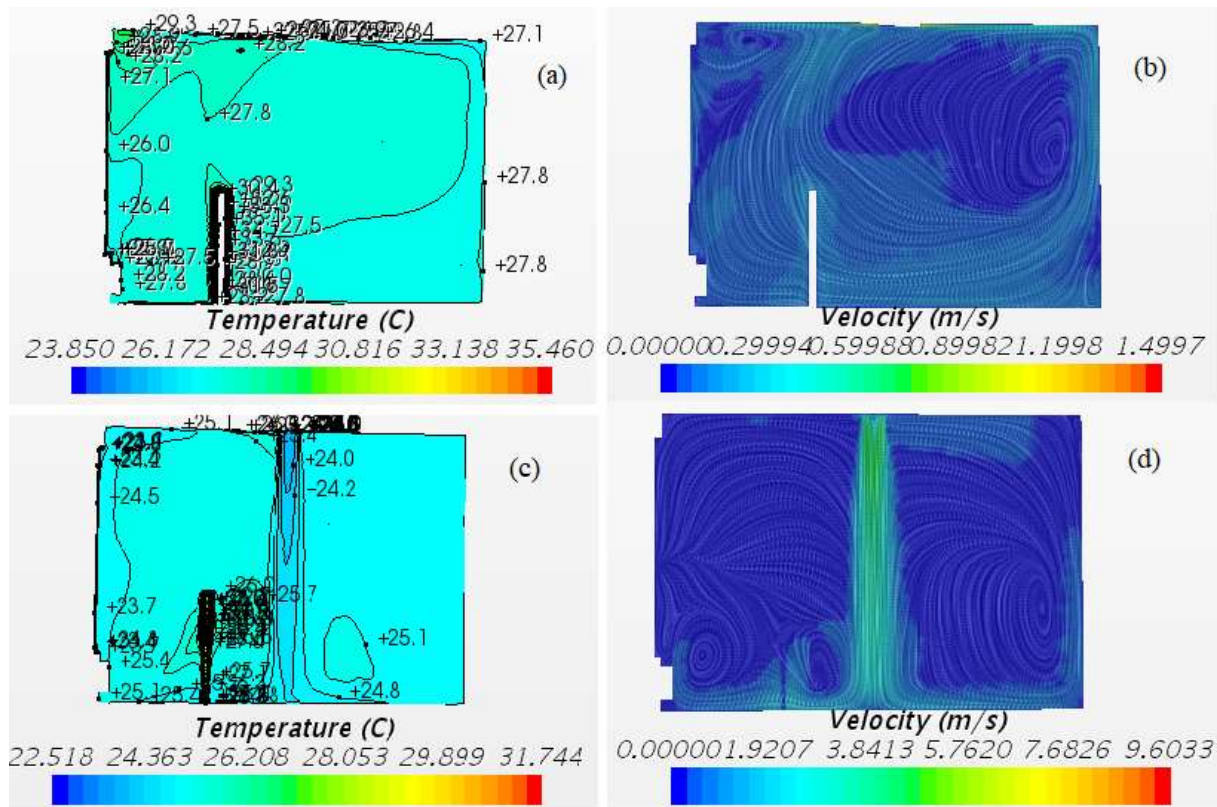


Figure 32. Temperature & velocity distribution along plane A for case 9 active diffuser (a) & (b) and perforated diffuser (c) & (d) .

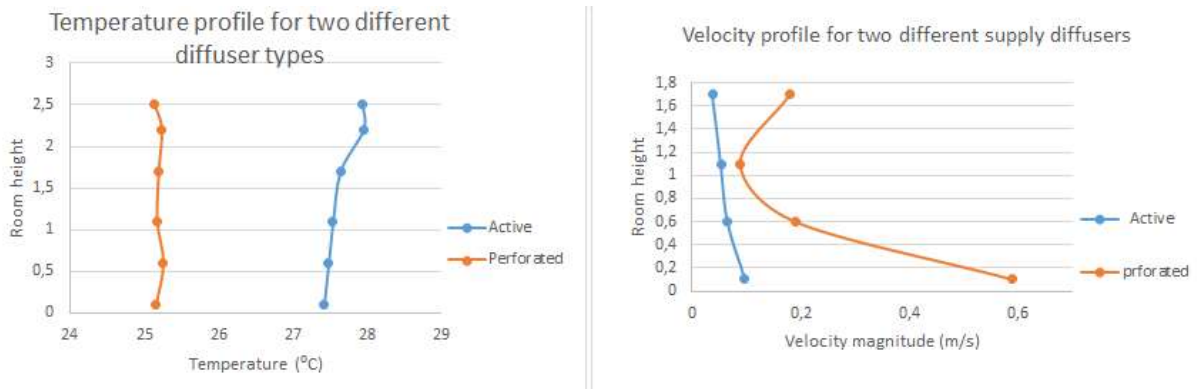


Figure 33: Vertical temperature profile and velocity profile for two different diffusers (case 9)

4.3.5. Evaluation of ventilation efficiency

This section presents ventilation efficiency interms of temperature effectiveness. For comparison of temperature effectiveness, case 9 has been considered and the calculated results based on equation 4 are 1.09, 0.62 for an active diffuser and perforated diffuser respectively. These results suggest an active supply diffuser has a better effective temperature effectiveness

than perforated diffuser. This is due to the reason that, there is some cold supply air leaving the exhaust with out being mixed with the room air in case of the supply air from perforated type diffuser.

4.4. Thermal comfort analysis

4.4.1. Operative temperature

The operative temperature has been calculated according to equation 7. The mean radiant temperature has been calculated from the surface average temperatures of the room, ceiling and window which has been recorded from the CFD result as shown in table 10, using equation 8. The view factor for the corresponding envelop surface has also been included in the table. The room average air temperature has also been recorded from the simulation result as volume average which is 27.6 °C. The calculated operative temperature and mean radiant temperature for case 1 are 27.6°C and 27.7°C respectively. The result shows the calculated operative temperature is higher than the recommended value in standard (Standard, 2005), for the heating season for a single office it should not be over 23 °C for category I. According to the conclusion made from the experimental study (Axel et al., 2015), a high operative temperature is an indication for at internal gain covers the heating demand in the heating seasons.

Table 10: Surface average temperatures for the room volume

Description	Surface temperature (°C)	View factors
Ceiling	27.66	0.2
Front wall	28	0.2
Rear wall	28.01	0.2
Left wall	27.66	0.1
Right wall	28.09	0.2
Window	25.86	0.1

The thermal comfort assessment has been conducted in terms of operative temperature, draught rate and vertical temperature difference (thermal stratification) for flow rate 177 m³/h at a supply air temperature of 24 °C. The results obtained from the CFD simulation is used to calculate Predictive Mean Vote (PMV) and the Predicted Percentage of Dissatisfied (PPD) to evaluate the thermal comfort.

The result obtained from the calculation using equation 5 and 6 is $PMV = 0.82$ and $PPD = 19.2\%$. The corresponding standard for category IV is ($PMV < -0.7$; or $+0.7 < PMV$ and $PPD > 15\%$) (Standard, 2005). However the result for perforated type diffuser shows that $PMV = -0.32$ and $PPD = 7.1\%$, which corresponds category II. This indicates that in terms of thermal comfort, perforated diffuser gives a better result.

4.4.2. Vertical temperature difference

The results obtained for vertical air temperature differences are 0.1°C between ankle level (0.1 m) and sitting height level (1.1 m) and 0.13°C between ankle level (0.1 m) and standing person height (1.7 m) in the office cubicle for volumetric flow rate of $177\text{ m}^3/\text{h}$. Whereas a gradient of 4.2°C corresponds to a percentage dissatisfied of 10%. This indicates the thermal stratification has been reduced for volumetric flow rate of $177\text{ m}^3/\text{h}$. Therefore there is no risk of thermal dissatisfaction due to vertical air temperature difference for this case even though the operative temperature is not in the comfort level.

4.4.3. Draught rate

The draught rate higher than 15% is considered as unacceptable (Standard, 2005). The results for average air temperature and average air velocity inside the room obtained from the CFD model simulation for $177\text{ m}^3/\text{h}$ at air supply temperature of 24°C was 27.6°C & 0.085 m/s . Therefore there is no thermal comfort problem due to draught rate (DR) inside the office occupant.

5. Conclusion and recommendation

The thesis investigates room air flow and temperature distributions of mixed ventilation, which is supplied by a ceiling mounted active diffuser. The study employs numerical simulation where the modelling is effected by standard procedures comprised of: developing geometry, meshing, boundary condition setting, defining physical properties, selection of physics models and simulation. The simulation program has been validated using the experimental data from previous study and selection of turbulence model has been conducted. The effects of supply air temperature and volumetric flow rate in the room air distribution have been studied. Moreover, effects of additional heating system and of different types of supply diffusers on the air flow distribution are parts of the present investigation. Therefore the following conclusions are drawn from this study:

- Simulation results show good agreement with experimental data with errors below 12 % for temperature profile and below 6 % for velocity profile for both $k-\varepsilon$ and $k-\omega$ turbulence models. The $k-\varepsilon$ model has been selected for the present study due to its better solution convergence for the simulations and it produces a velocity profile of the experimental data.
- The parametric analysis suggests that the supply air temperature does not influence the air flow velocity and the vertical temperature gradient in the room for flow rate of 126 m³/h and flow rate of 76 m³/h. However, for flow rate of 51 m³/h an increase in supply air temperature increases the vertical temperature gradient.
- The parametric analysis also suggests that the air flow distribution inside the room is affected by the outdoor temperature of -10 °C due to the heat transfer between the outdoor environment and the façade/window. In addition to this, the results suggest an increase in supply air temperature with decreasing supply air flow rate reduces the vertical temperature gradient (thermal stratification for flow rate 51 m³/h) as a result of the heat transfer (loss) with the outdoor environment.
- Variation in volumetric flow rate with constant supply air temperature impacts the airflow inside the room. For all cases, the vertical temperature gradient increases with increasing height. Therefore, the results suggest that room air temperature increases with a decrease in volumetric flow rate.
- The simulation result has shown that perforated supply diffuser creates a better room temperature for the occupants. However, it generates a high velocity in an occupied zone, which might have a high potential of draught risk to the occupants. Thermal

comfort in terms of PMV and PPD evaluation has also shown that perforated diffuser creates a better thermal environment and the calculated results are in the recommended standard level.

In summary, the validated CFD technique with k- ϵ turbulent model can be used for designing of the temperature and velocity distribution of a high energy efficient office buildings using mixed ventilation systems with ceiling mounted active diffuser. In conclusion, it is recommended

- To investigate the ventilation efficiency for the active supply diffuser in terms of contaminant removal in the future work.
- Further investigation of the real effects of the moving slots of the active supply diffusers on the flow velocity and temperature distribution.

- Amai, H., & Novoselac, A. (2016). Experimental study on air change effectiveness in mixing ventilation. *Building and Environment*, *109*, 101-111.
doi:<https://doi.org/10.1016/j.buildenv.2016.09.015>
- Axel, C., MYSEN, M., & THUNSHELLE, K. (2015). *CAN DEMAND CONTROLLED VENTILATION REPLACE SPACE HEATING IN OFFICE BUILDINGS WITH LOW HEATING DEMAND?* SINTEF, Oslo, Norway , Oslo and Akershus University College of Applied Sciences. Oslo, Norway.
- Buratti, C., Palladino, D., & Moretti, E. (2017). Prediction Of Indoor Conditions And Thermal Comfort Using CFD Simulations: A Case Study Based On Experimental Data. *Energy Procedia*, *126*, 115-122.
doi:<https://doi.org/10.1016/j.egypro.2017.08.130>
- Cao, G., Awbi, H., Yao, R., Fan, Y., Sirén, K., Kosonen, R., & Zhang, J. (2014). A review of the performance of different ventilation and airflow distribution systems in buildings. *Building and Environment*, *73*, 171-186.
doi:<https://doi.org/10.1016/j.buildenv.2013.12.009>
- Catalina, T., Virgone, J., & Kuznik, F. (2009). Evaluation of thermal comfort using combined CFD and experimentation study in a test room equipped with a cooling ceiling. *Building and Environment*, *44*(8), 1740-1750. doi:10.1016/j.buildenv.2008.11.015
- Engineers, P. (2011). Engineering guid air distribution In P. i. Lmtd. (Ed.), (pp. 14).
- Gan, H. B. A. a. G. (1993). *Evaluation of the overall performance of room air distribution* Paper presented at the Indoor Air Helsinki, Finland.
- GANGISETTI, K. (2010). *PREDICTION OF ROOM AIR DIFFUSION FOR REDUCED DIFFUSER FLOW RATES*. (MSc. MASTER OF SCIENCE), Texas A&M University, USA.
- Iverson, J. M. (2013). *Computational Fluid Dynamics Validation of Buoyant Turbulent Heat transfer* (Msc. Masters thesis), Utah State University (1)
- Jones, W. P. (1997). Air Distribution. In *Air Conditions Application and Design* (2nd ed., pp. 23). 2 Park Square, Milton Park, Abingdon, Oxon OX144RN , 711 Third Avenue, New York, NY10017, USA: Routledge
- Kharagpur, T. Space Air Distribution
- LINDVENT. Active supply diffuser. In Lindvent (Ed.).
- Mike Kuron, M. S. M. E. (2015). 3 Criteria for Assessing CFD Convergence.
- Miroshnichenko, I. V., & Sheremet, M. A. (2018). Turbulent natural convection heat transfer in rectangular enclosures using experimental and numerical approaches: A review. *Renewable and Sustainable Energy Reviews*, *82*, 40-59.
doi:<https://doi.org/10.1016/j.rser.2017.09.005>

- Nielsen, P. V. (1988). The selection of Turbulence Models for Prediction of Room Airflow *R9828*, 16
- Nielsen, P. V. (1995). *Lecture Notes on Mixing Ventilation*
- Ning, L. (2015). *Comparison between three different CFD software and numerical simulation of an ambulance hall*. (Msc), KTH school of Industrial Engineering and Management Stockholm.
- Qasim, H. H., Sabah, T. A., & Ala'a Abbas, M. (2014). Numerical Simulation of Air Velocity and Temperature Distribution in an Office Room ventilated by Displacement Ventilation System. *Scientific & Engineering Research* 5(4), 11.
- Qingyan, C., & Srebric, J. (2002). A Procedure for Verification, Validation, and Reporting of Indoor Environment CFD Analyses. *HVAC&R Research*, 8, 17.
- RISBERG, D., WESTERLUND, L., & I. HELLSTRÖM, J. G. CFD SIMULATION OF INDOOR CLIMATE IN LOW ENERGY BUILDINGS COMPUTATIONAL SETUP. 15.
- Standard, N. (2005). Ergonomics of the thermal environment Analytical determination interpretation of thermal comfort using calculation of PMV and PPD indices and local thermal criteria. In *ISO 7730:2005* (pp. 64). B-1050 Brussels: European Committee for Standardization
- Standard, N. (2014). Inneklimaparametere for dimensjonering og vurdering av bygningers energiytelse inkludert inneluftkvalitet, termisk miljø, belysning og akustikk (Indoor environmental input parameters for design and assessment of energy performance of buildings addressing indoor air quality, thermal environment, lighting and acoustics). In (pp. 64).
- STARCCM+. (2017). Users Guide (Version 12).
- Swegon. Perforated supply diffuser In.
- Syed, A. (2012). *Advanced Building Technologies for Sustainability*. Somerset, UNITED STATES: John Wiley & Sons, Incorporated.
- Tomasi, R., Krajčik, M., Simone, A., & Olesen, B. W. (2013). Experimental evaluation of air distribution in mechanically ventilated residential rooms: Thermal comfort and ventilation effectiveness. *Energy and Buildings*, 60, 28-37.
doi:<https://doi.org/10.1016/j.enbuild.2013.01.003>
- Union, E. (2012). Energy Performance of Buildings Directive. In (pp. 44). Dublin: The Stationary Office
- Versteeg, H. K., & Malalasekera, W. (2007). *Introduction to Computational Fluid Dynamics The finite volume method* (2nd edition ed. Vol. 2). Edinburgh Gate, Harlow, Essex CM20 2JE , England: Pearson Education Limited.

Appendix 1: Active supply air diffuser

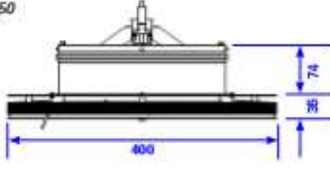
Product description
TTC – Active supply air diffuser

Technical specifications TTC

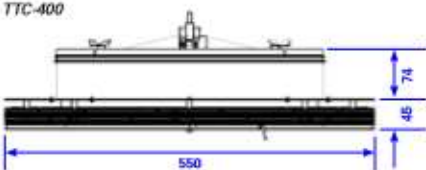
General

Dimensions (mm)
For dimensions of plenum boxes and diffuser adapters, see the product descriptions for HTK, HTR, DAB and DAS.

TTC-250



TTC-400



Material
Powder coated steel plate

Net weight
TTC-250: 5.6 kg
TTC-400: 8.5 kg

Paint colour
RAL 9003 (Gloss 30) as standard.
Other colours may be specially ordered; please state RAL number.

Temperature limits
Operation: 10°C to 30°C; <85% RF
Storage: -20°C to 50°C; <90% RF

Miscellaneous
Supplied with mounted and pre-connected 14-conductor cable (connects to connection box CBX) of the length stated when ordering.
Standard length of 14-conductor cable: 1 m
Maximum length of 14-conductor cable: 10 m

Electrical system

Supply voltage
24 VAC

Capacity
2 VA at rest
4 VA during adjustment (c 50–100 h/year)

CE marking
Complies with EMC and the Low Voltage Directive

Occupancy detection

Occupancy detector
The diffuser has an integral occupancy detector (passive IR detector).

Coverage angles
See product description for XPIR.

Duct temperature measurement

Temperature sensor
Sensor with thermistor of NTC type.

Accuracy
Temperature ± 0.5 K

Room temperature measurement

Temperature sensor
Sensor with thermistor of NTC type.

Accuracy
Temperature ± 0.5 K

Pressure and air flow measurement

Pressure and air flow sensor
TTC is equipped with the sensor, integrated in the diffuser.

Interval
TTC-250: 10-120 Pa
TTC-400: 10-120 Pa
If a higher pressure range is needed (max 250 Pa) please state this when ordering

Accuracy
 $\pm 5\%$ or a minimum of ± 3 Pa

Air flow adjustment

Interval
TTC-250: 3-65 l/s
TTC-400: 5-100 l/s

Tolerance
 $\pm 5\%$ or minimum ± 2 l/s (correct measurement does not require any preceding straight stretch)

Performance
Maximum change adjusted within c. 2 min.

Connections (Via connection box CBX)

- 2 x 24 VAC measurement + communication loop (CAN)
- 2 x 0-10 VDC analogue in
- 1 x control signal to relay on lighting card CBR.
- 1 x 5 VDC input for push button with lighting control.
- 2 x 0-10 VDC analogue out
- 1 x 24 VAC, TRIAC (intended for valve actuator).


Connections (Direct on diffuser)

- 1 x IR unit

Pressure, flow and sound levels
See page 5.

WWW.LINDINVENT.SE

TTC_A30_PB28_HPT45_eng

LINDINVENT 

4(6)

Figure 34: Product description for active supply diffuser

Appendix 2: Project execution plan

Table 11: project execution plan for the master's thesis

		Execution plan for master thesis																											
		January					February					March					April					May					June		
Description		W1	W2	W3	W4	W5	W6	W7	W8	W9	W10	W11	W12	W13	W14	W15	W16	W17	W18	W19	W20	W21	W22	W23	W24	W25			
		Analyzing and defining the problem statement		Green	Green	Green	Green																						
Litreature review			Yellow	Yellow	Yellow	Yellow	Yellow	Yellow	Yellow	Yellow	Yellow	Yellow	Yellow	Yellow	Yellow	Yellow	Yellow	Yellow	Yellow	Yellow	Yellow	Yellow	Yellow	Yellow	Yellow	Yellow			
Miles meeting							Blue																						
Understanding STAR CCM+			Dark Blue	Dark Blue	Dark Blue	Dark Blue	Dark Blue	Dark Blue																					
Developing model and starting simulating							Brown	Brown	Brown	Brown	Brown	Brown	Brown	Brown	Brown	Brown	Brown	Brown	Brown	Brown	Brown	Brown	Brown	Brown	Brown	Brown			
Compare results with experimental data													Brown																
Miles meeting															Blue														
Simulation of the model for different conditions								Green	Green	Green	Green	Green	Green	Green	Green	Green	Green	Green	Green	Green	Green	Green	Green	Green	Green	Green			
Report writign																					Purple	Purple	Purple	Purple	Purple	Purple			
Editing and finalizing the report																					Blue	Blue	Blue	Blue	Blue	Blue			
Submission of the thesis																								Orange					
Presentation and evaluation																										Dark Blue			

Appendix 3: Velocity contour for different flow rates at outdoor temperature -1.8 °C

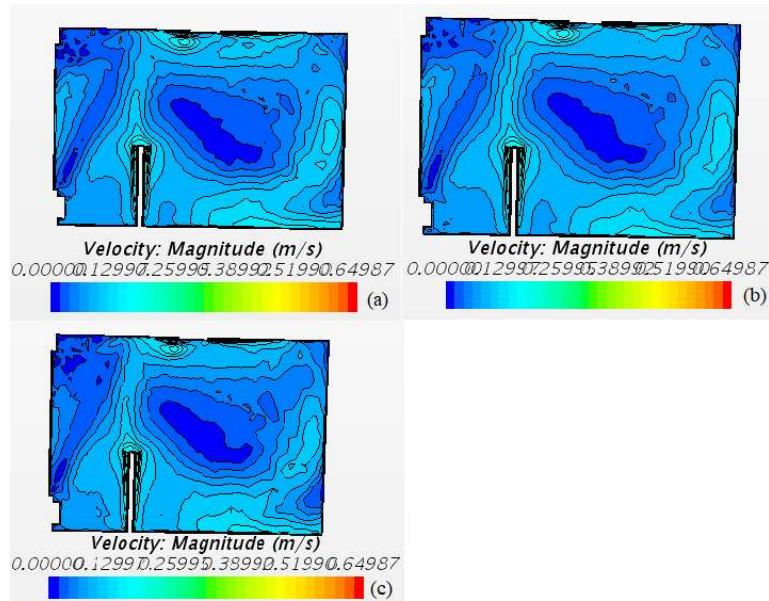


Figure 35: Velocity contour for flow rate of 76 m³/h at supply air temperatures (a) 24 °C, (b) 26 °C and (c) 28 °C at outdoor temperature of -1.8 °C

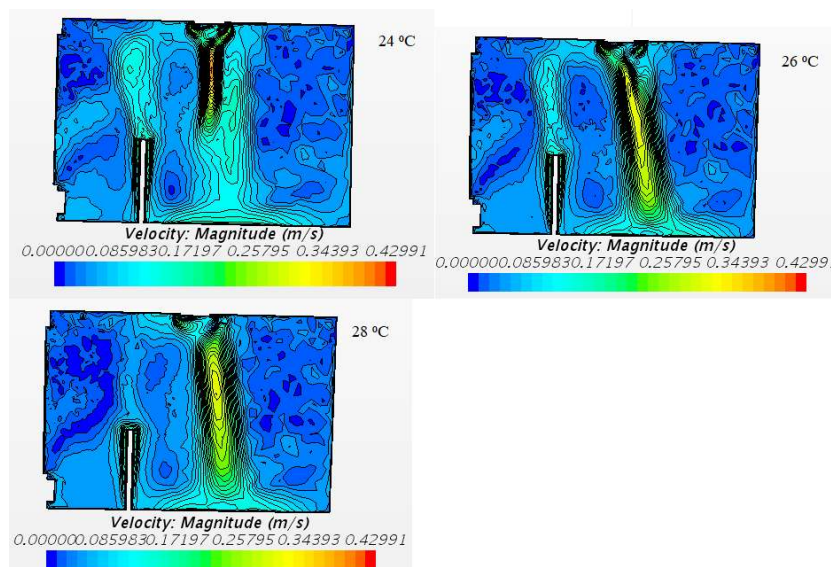


Figure 36: Velocity contour for flow rate of 51 m³/h at supply air temperatures 24 °C, 26 °C and 28 °C at outdoor temperature of -1.8 °C

Appendix 4 – Temperature and velocity profiles for different flow rates

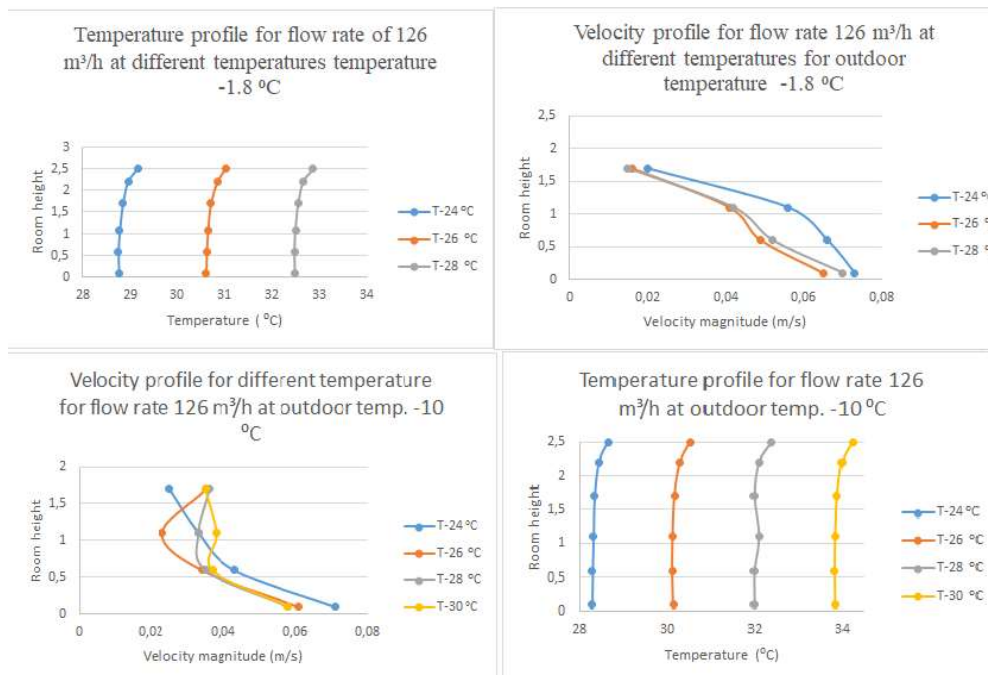


Figure 37: Temperature and velocity profile for flow rates 126 m³/h different supply temperature for outdoor temperature of – 1.8 °C and 10 °C.

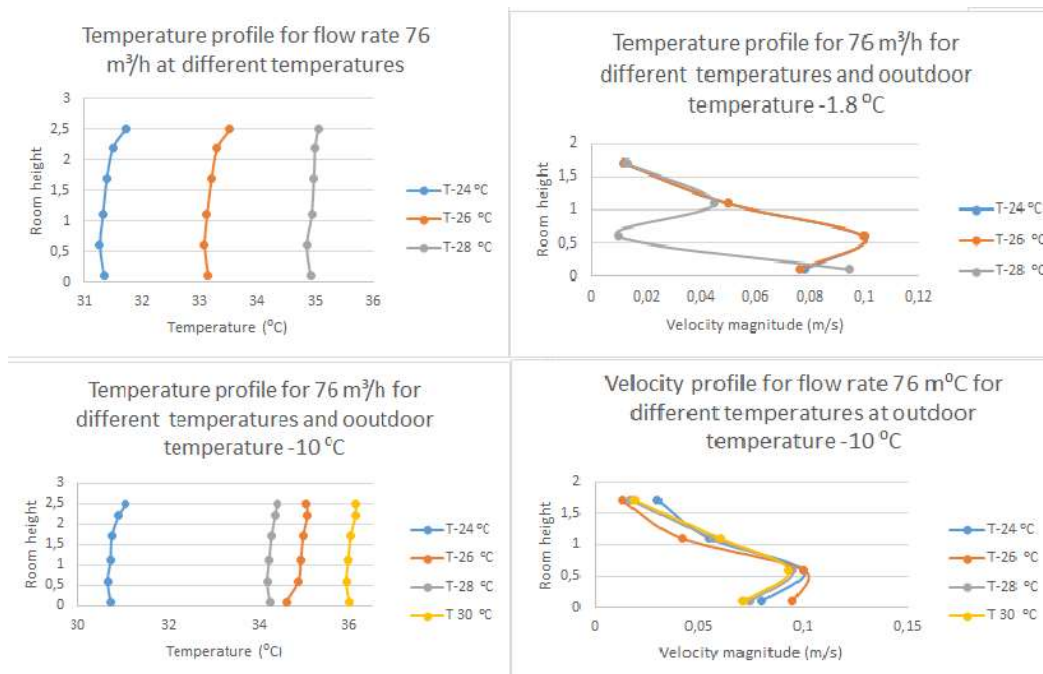


Figure 38: Temperature and velocity profile for flow rate 76 m³/h different supply temperature for outdoor temperature of – 1.8 °C and 10 °C.

Appendix 5 : Velocity contours for different flow rates at outdoor temperature -10 °C

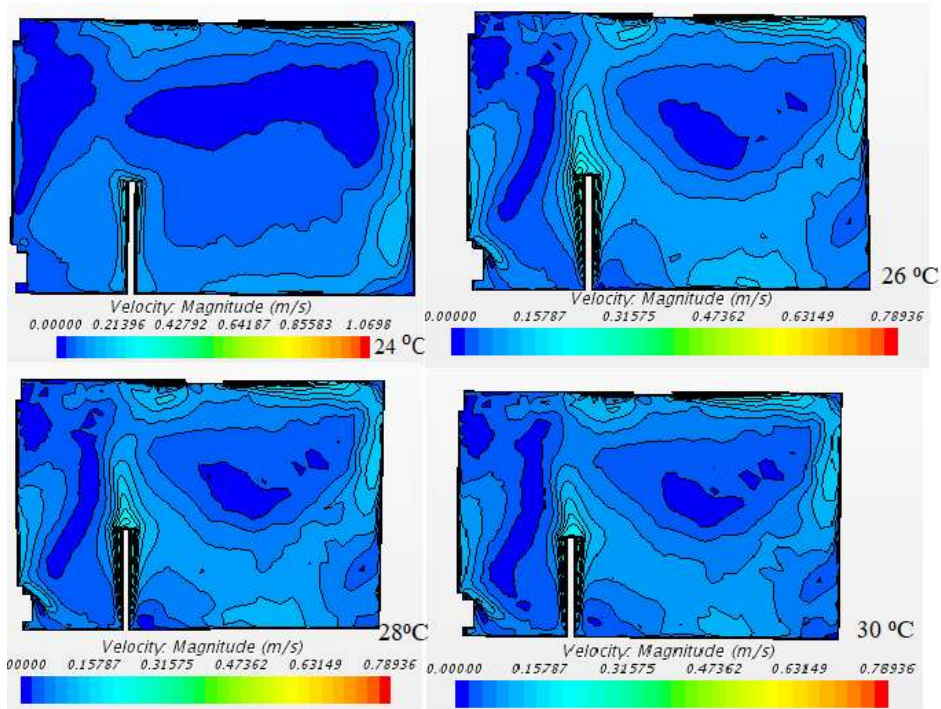


Figure 39: Velocity contour of flow rate 126 m³/h for different supply air temperatures at outdoor temperature of -10 °C.

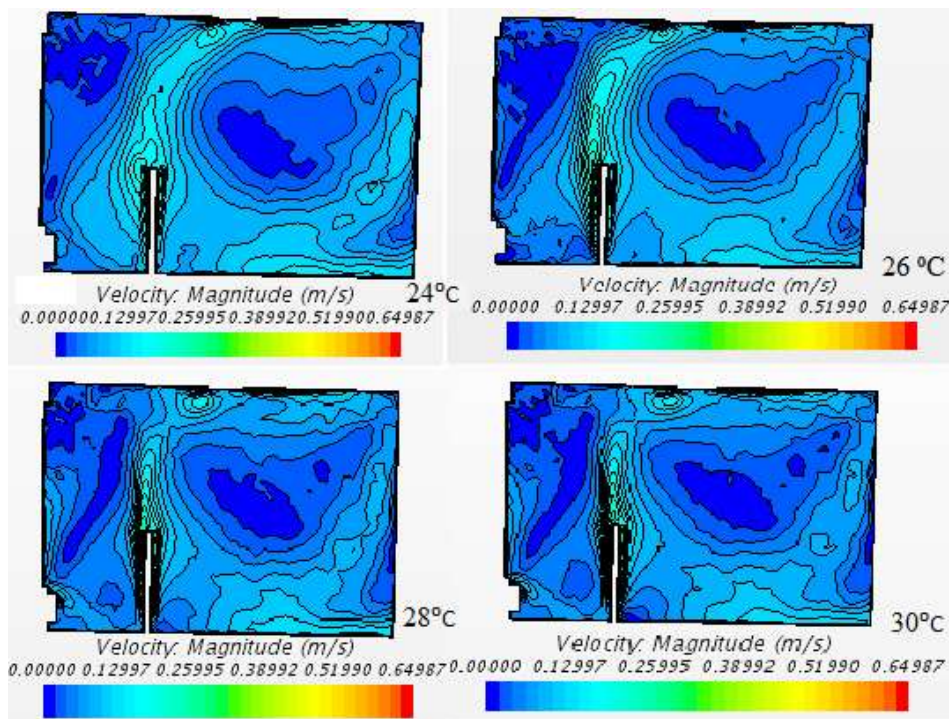


Figure 40: Velocity contour of flow rate 76 m³/h for different supply air temperatures at outdoor temperature of -10 °C.

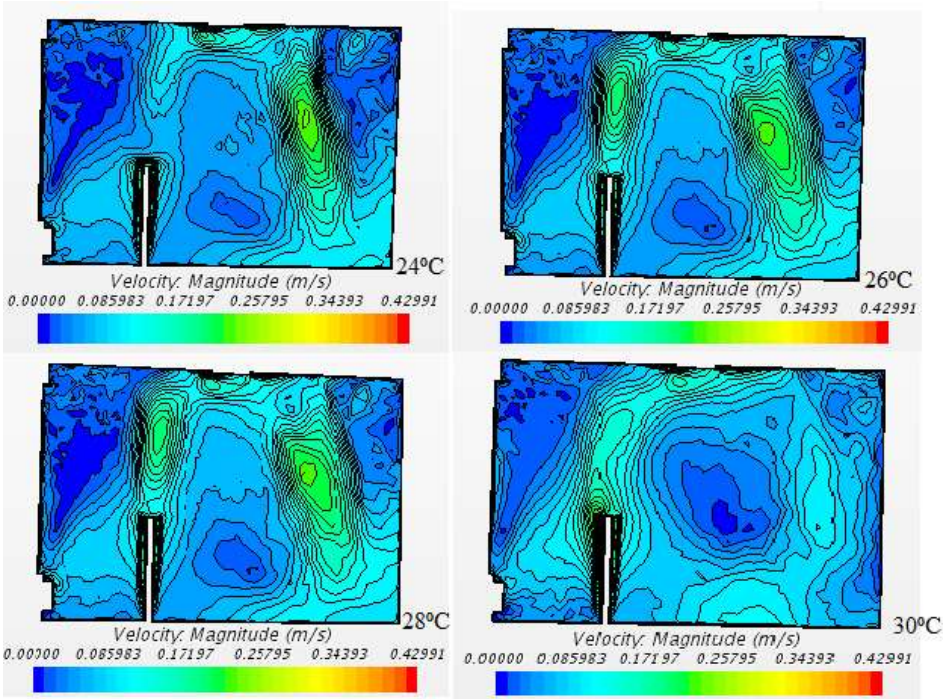


Figure 41: Velocity contour of flow rate 51 m³/h for different supply air temperatures at outdoor temperature of -10 °C.